Collective Long-Lived Zero-Quantum Coherences in Aliphatic Chains

Kirill F. Sheberstov, Anna Sonnefeld, Geoffrey Bodenhausen

Collective Long-Lived Zero-Quantum Coherences in Aliphatic Chains

Kirill F. Sheberstov*, Anna Sonnefeld, and Geoffrey Bodenhausen*

Laboratoire des biomolécules, LBM, Département de chimie, École normale supérieure,

PSL University, Sorbonne Université, CNRS, 75005 Paris, France

To be resubmitted to J. Chem. Phys.

Manuscript Number: JCP24-AR-00143

*Corresponding authors

kirill.sheberstov@ens.psl.eu

geoffrey.bodenhausen@ens.fr

KS's ORCID: 0000-0002-3520-6258

AS's ORCID: 0000-0002-2194-8357

GB's ORCID: 0000-0001-8633-6098

Abstract

In nuclear magnetic resonance (NMR), long-lived coherences (LLCs) constitute a class of zero-quantum (ZQ) coherences that have lifetimes that can be longer than the relaxation lifetimes T_2 of transverse magnetization. So far, such coherences have been observed in systems with two coupled spins with spin quantum numbers I = ½, where a term $|S_0\rangle\langle T_0| + |T_0\rangle\langle S_0|$ in the density operator corresponds to a coherent superposition between the singlet $|S_0\rangle$ and the central triplet $|T_0\rangle$ state. Here we report on the excitation and detection of collective long-lived coherences in AA'MM'XX' spin systems in molecules containing a chain of at least three methylene (-CH_2-) groups. Several variants of excitation by polychromatic spin-lock induced crossing (poly-SLIC) are introduced that can excite a non-uniform distribution of the amplitudes of terms such as $|S_0S_0T_0\rangle\langle S_0S_0T_0|$, $|S_0T_0S_0\rangle\langle S_0T_0S_0|$, and $|T_0S_0S_0\rangle\langle T_0S_0S_0|$. Once the radio frequency (RF) fields are switched off, these are not eigenstates, leading to ZQ precession involving all 6 protons, a process that can be understood as a propagation of spin order along the chain of -CH_2- groups, before their reconversion into observable magnetization by a second poly-SLIC pulse that can be applied to any one or several of the CH_2 groups. In the resulting 2D spectra, the ω_2 domain shows SQ spectra with the chemical shifts of the CH_2 groups irradiated during the reconversion, while the ω_1 dimension shows ZQ signals in absorption mode with linewidths on the order of 0.1 Hz that are not affected by the inhomogeneity of the static magnetic field, but can be broadened by chemical exchange as occurs in drug screening. The ZQ frequencies are primarily determined by differences ΔJ between vicinal J-couplings.

Key words

Long-Lived Coherences, Spin-Chains, Zero-Quantum Spectroscopy, Polychromatic Spin-Lock Induced Crossings, Drug Screening.

Introduction

Spin symmetry plays a pivotal role for relaxation properties in nuclear magnetic resonance (NMR). Population imbalances between states belonging to different irreducible representations of the spin permutation group are known as long-lived states (LLSs), since their lifetimes T_{LLS} can be significantly longer than the longitudinal ('spin-lattice') relaxation time constant T_1 [1–5]. On the other hand, zero-quantum coherences between states belonging to different irreducible representations, known as long-lived coherences (LLCs), can have lifetimes T_{LLC} that may be longer than the relaxation time constant T_2 of transverse magnetization. For a pair of spins with I = ½, an LLC corresponds to a coherent superposition between the singlet state $S_0 = \frac{1}{\sqrt{2}}[\alpha\beta - \beta\alpha]$ and the central triplet state ($T_0 = \frac{1}{\sqrt{2}}[\alpha\beta + \beta\alpha]$). Such LLCs were first described for a pair of chemically inequivalent spins evolving at very low static magnetic fields [6], where they can be excited by extremely low frequency (ELF) irradiation, using electromagnetic fields that oscillate in the audio range. The excitation and observation of LLCs was soon extended to higher static fields, where their evolution can be "sustained" by a strong RF field that suppresses the differences between chemical shifts and hence forces the pair of spins to be chemically equivalent [7]. Similar LLCs can also be observed in strongly coupled spin pairs without sustaining by RF fields [8]. The lifetime T_{LLC} can be longer than T_2 by a factor $\kappa = T_{\mathrm{LLC}}/\mathrm{T}_2 \leq 3$ for relaxation caused by dipolar interactions in the extreme narrowing regime (i.e., for small molecules such as drugs in non-viscous liquids) and $\kappa \leq 9$ in the slow motion regime [9]. Experimentally, the homogeneous linewidths in LLC spectra were observed to be up to 2.6 times narrower than in single-quantum (SQ) spectra in the extreme narrowing regime, and up to 4.6 times narrower in the slow motion regime [8,9]. Since LLCs constitute a particular class of zero-quantum coherences (ZQCs), they benefit from the attractive property that they are insensitive to the inhomogeneity of the static magnetic field [10–13]. On the other hand, zero-quantum (ZQ) linewidths can be exquisitely sensitive to exchange broadening as may occur in drug screening experiments. In heteronuclear systems comprising, say, ^{1}H and ^{13}C, LLCs can be observed at zero- or ultralow-fields [14,15].

Here we expand our work [16] on aliphatic chains in achiral molecules at high fields. We consider the case of molecules containing three CH_2 groups, each group having a distinct chemical shift. The geminal protons of each group are chemically equivalent but magnetically inequivalent, thus forming an AA'MM'XX' spin system in Pople's notation [17]. The dominant intra-pair dipole-dipole couplings $D_{\mathrm{AA'}}$, $D_{\mathrm{MM'}}$, and $D_{\mathrm{XX'}}$ do not affect relaxation of LLSs for reasons of symmetry, while out-of-pair dipole-dipole couplings such as D_{AM}, $D_{\mathrm{AM'}}$, etc. have much smaller contributions to their relaxation rates because of the larger internuclear distances. By contrast, both intra-pair and out-of-pair dipole-dipole couplings may contribute to LLC relaxation [8,9]. Relaxation of both LLSs and LLCs is affected by dissolved oxygen [18,19] and other paramagnetic species [20].

The application of various mono- or polychromatic variants [16] of spin-lock induced crossing (SLIC) [21] to such systems generates population imbalances between states of different symmetry. Within each CH_2 group, *scalar two-spin order* can be expressed by a scalar product $\hat{\boldsymbol{I}}^A \cdot \hat{\boldsymbol{I}}^{A'} = \left(\hat{I}_x^A \cdot \hat{I}_x^{A'} + \hat{I}_y^A \cdot \hat{I}_y^{A'} + \hat{I}_z^A \cdot \hat{I}_z^{A'}\right) = \frac{1}{4}\left(\left|T_{+1}^{AA'}\right\rangle\left\langle T_{+1}^{AA'}\right| + \left|T_0^{AA'}\right\rangle\left\langle T_0^{AA'}\right| + \left|T_{-1}^{AA'}\right\rangle\left\langle T_{-1}^{AA'}\right| - 3\left|S_{+1}^{AA'}\right\rangle\left\langle S_{+1}^{AA'}\right|\right)$. If all two-spin order terms associated with the three geminal spin pairs (e.g., $\hat{\boldsymbol{I}}^A \cdot \hat{\boldsymbol{I}}^{A'}$, $\hat{\boldsymbol{I}}^M \cdot \hat{\boldsymbol{I}}^{M'}$ and $\hat{\boldsymbol{I}}^X \cdot \hat{\boldsymbol{I}}^{X'}$) could be excited uniformly, the resulting state would be a *stationary* eigenstate of the free precession Hamiltonian, by essence time-independent, apart from slow relaxation. If we excite these scalar two-spin terms with different amplitudes, the resulting state can comprise both LLSs (diagonal terms in the density matrix represented in the eigenbasis of the free precession Hamiltonian) and LLCs (off-diagonal elements in the same eigenbasis). Our earlier work [16] focused attention on the slowly-decaying LLS, whereas the present paper provides a detailed description of the rapidly-oscillating LLCs.

We have found that to describe the behavior of the LLCs in 6-spin systems, one should consider singlet-triplet product states such as $|T_0^{AA'}S_0^{MM'}S_0^{XX'}\rangle$, $|S_0^{AA'}T_0^{MM'}S_0^{XX'}\rangle$, $|S_0^{AA'}S_0^{MM'}T_0^{XX'}\rangle$. In practice, the amplitudes of these product states, i.e., the projections of the density operator onto terms such as $|T_0^{AA'}S_0^{MM'}S_0^{XX'}\rangle\langle T_0^{AA'}S_0^{MM'}S_0^{XX'}|$, etc., are usually not uniform along the chain. The resulting state is therefore *not* an eigenstate of the free precession Hamiltonian and will evolve, a process that we shall refer to as *propagation*. When these LLCs involve more than two spins, they will be called *collective*.

Here, we present experiments which aim to enhance the *non-uniformity* of the amplitudes of the relevant singlet-triplet product states and thereby increase the amplitude of the collective LLCs. This can be achieved by suitable poly-SLIC excitation schemes. We also explore the effects of *selective decoupling* of one or several of the CH_2 groups, either during the excitation of LLSs and LLCs, or during the evolution time t_1. Selective decoupling, which can be achieved by applying a weak RF field with an amplitude that must differ from the SLIC condition, in effect allows one to cut the length of a chain of coupled CH_2 groups, as if one could tailor the length of the molecule at will, as used to be the realm of alchemists.

After excitation, the spin order propagates along the chain. The velocity of the propagation, or, equivalently, the precession frequency of the LLCs, is determined by energy differences between eigenstates, which in turn are primarily determined by differences ΔJ between vicinal couplings. ZQ spectra are obtained by a real Fourier transformation of the time-dependence of signals derived from LLCs by reconversion SLIC sequences. At the end of the evolution interval t_1, after filtration by a T_{00} filter, various SLIC methods can be used to *project* chosen constituents of the density operator onto observable magnetization. Our method has the potential to be generalized to aliphatic chains of arbitrary length, provided the chemical shifts are not degenerate.

Similar experiments conducted on ABXY systems in *chiral* molecules by DeVience et al. [22] showed that the propagation of the expectation values of the singlet-triplet product states between two CH_2 groups can be facilitated by exploiting differences between vicinal *J*-couplings in the presence of a sustaining (spin-locking) RF irradiation. In this paper, we focus on *achiral* molecules containing aliphatic chains, and the propagation takes place during free evolution, without requiring any RF fields.

There are analogies between our NMR methods and the concept of spin waves that has been discussed since the 1920's to elucidate the physics of ferromagnetism, conductors, and semiconductors, where the motions of unpaired electrons are constrained by a periodic potential in solids. Subsequent theories have given rise to the emergence of the Lenz-Ising model for ferromagnetism [23,24] and to Bloch's theorem that demonstrates how the eigenstates of Schrödinger's equation in a periodic potential are plane waves modulated by periodic functions [25]. While electron spin waves became a classical textbook problem [26], they have so far rarely been considered in solution-state NMR, although the propagation of magnetization along a chain of scalar-coupled nuclei has been observed under spin-locking conditions [27–30]. The proton spin systems in aliphatic chains -$(CH_2)_n$- can be considered as examples of one-dimensional lattices of magnetically inequivalent pairs of coupled spins of finite length [31]. In each -(CH_2)-subsystem, the pair of states $|S_0\rangle$ and $|T_0\rangle$ spans a two-level subsystem that can be described by a fictitious spin with spin quantum number I = 1/2. Such a *spin-chain* bears analogies to one-dimensional chains of unpaired electron spins with I = 1/2 that have been described for arbitrary values of *n* [26].

Theory

Full spin Hamiltonian of the AA'MM'XX' spin system

In this work we shall focus attention on aliphatic chains with *n* = 3 consecutive methylene groups ($R-\mathrm{CH}_2^{AA'}-\mathrm{CH}_2^{MM'}-\mathrm{CH}_2^{XX'}-R'$). The full spin Hamiltonian of aliphatic protons in achiral molecules with magnetically inequivalent (although chemically equivalent) pairs of protons can be written as:

$$\hat{H} = \hat{H}_Z + \hat{H}_J,$$

$$\hat{H}_Z = \nu_A\left(\hat{I}_z^A + \hat{I}_z^{A'}\right) + \nu_M\left(\hat{I}_z^M + \hat{I}_z^{M'}\right) + \nu_X\left(\hat{I}_z^X + \hat{I}_z^{X'}\right),$$

$$\hat{H}_J = \hat{H}_J^{geminal} + \hat{H}_J^{vicinal} + \hat{H}_J^{long-range}, \text{ where} \tag{1}$$

$$\hat{H}_J^{geminal} = J_{AA'}\hat{\boldsymbol{I}}^A \cdot \hat{\boldsymbol{I}}^{A'} + J_{MM'}\hat{\boldsymbol{I}}^M \cdot \hat{\boldsymbol{I}}^{M'} + J_{XX'}\hat{\boldsymbol{I}}^X \cdot \hat{\boldsymbol{I}}^{X'},$$

$$\hat{H}_J^{vicinal} = \frac{1}{2}\Sigma J_{AM}\left(\hat{\boldsymbol{I}}^A \cdot \hat{\boldsymbol{I}}^M + \hat{\boldsymbol{I}}^A \cdot \hat{\boldsymbol{I}}^{M'} + \hat{\boldsymbol{I}}^{A'} \cdot \hat{\boldsymbol{I}}^M + \hat{\boldsymbol{I}}^{A'} \cdot \hat{\boldsymbol{I}}^{M'}\right) +$$

$$\frac{1}{2}\Sigma J_{MX}\left(\hat{\boldsymbol{I}}^{M}\cdot\hat{\boldsymbol{I}}^{X}+\hat{\boldsymbol{I}}^{M}\cdot\hat{\boldsymbol{I}}^{X\prime}+\hat{\boldsymbol{I}}^{M\prime}\cdot\hat{\boldsymbol{I}}^{X}+\hat{\boldsymbol{I}}^{M\prime}\cdot\hat{\boldsymbol{I}}^{X\prime}\right)+$$

$$\frac{1}{2}\Delta J_{AM}\left(\hat{\boldsymbol{I}}^{A}\cdot\hat{\boldsymbol{I}}^{M}-\hat{\boldsymbol{I}}^{A}\cdot\hat{\boldsymbol{I}}^{M'}-\hat{\boldsymbol{I}}^{A'}\cdot\hat{\boldsymbol{I}}^{M}+\hat{\boldsymbol{I}}^{A\prime}\cdot\hat{\boldsymbol{I}}^{M\prime}\right)+$$

$$\frac{1}{2}\Delta J_{MX}\left(\hat{\boldsymbol{I}}^{M}\cdot\hat{\boldsymbol{I}}^{X}-\hat{\boldsymbol{I}}^{M}\cdot\hat{\boldsymbol{I}}^{X'}-\hat{\boldsymbol{I}}^{M'}\cdot\hat{\boldsymbol{I}}^{X}+\hat{\boldsymbol{I}}^{M\prime}\cdot\hat{\boldsymbol{I}}^{X\prime}\right),$$

$$\widehat{H}_{J}^{long-range}=\frac{1}{2}\Sigma J_{AX}\left(\hat{\boldsymbol{I}}^{A}\cdot\hat{\boldsymbol{I}}^{X}+\hat{\boldsymbol{I}}^{A}\cdot\hat{\boldsymbol{I}}^{X'}+\hat{\boldsymbol{I}}^{A'}\cdot\hat{\boldsymbol{I}}^{X}+\hat{\boldsymbol{I}}^{A'}\cdot\hat{\boldsymbol{I}}^{X'}\right)+$$

$$\frac{1}{2}\Delta J_{AX}\left(\hat{\boldsymbol{I}}^{A}\cdot\hat{\boldsymbol{I}}^{X}-\hat{\boldsymbol{I}}^{A}\cdot\hat{\boldsymbol{I}}^{X'}-\hat{\boldsymbol{I}}^{A'}\cdot\hat{\boldsymbol{I}}^{X}+\hat{\boldsymbol{I}}^{A\prime}\cdot\hat{\boldsymbol{I}}^{X\prime}\right).$$

here all terms are expressed in units of Hz, ν_i stand for chemical shifts, J_{ij} denote *J*-couplings, $\Sigma J_{AM} = J_{AM} + J_{AM\prime}$ and $\Delta J_{AM} = J_{AM} - J_{AM\prime}$, etc. Bold operators represent vector operators, e.g., $\hat{\boldsymbol{I}}^{A} = \left(\hat{I}_x^A, \hat{I}_y^A, \hat{I}_z^A\right)$.

The two protons of a CH_2 group in such a system are *magnetically* inequivalent if the vicinal couplings to protons in a neighboring CH_2 group are not equal:

$$\Delta J_{AM} = |J_{AM} - J_{AM\prime}| = |J_{A\prime M\prime} - J_{A\prime M}| \neq 0. \tag{2}$$

$$\Delta J_{MX} = |J_{MX} - J_{MX\prime}| = |J_{M\prime X\prime} - J_{M\prime X}| \neq 0. \tag{3}$$

The condition of magnetic inequivalence can only be fulfilled if the populations of the three rotamers with respect to a rotation about the bond between the two neighboring carbon atoms are *not* equal, i.e., if the three potential wells have unequal depths [39,40]. This aspect will be discussed in more detail in a forthcoming paper.

All terms in the Hamiltonian of Eq. (1) commute with the operator representing simultaneous intra-pair permutation of all pairs of geminal protons:

$$\hat{p}_{global} = \hat{p}^{AA\prime}\cdot\hat{p}^{MM\prime}\cdot\hat{p}^{XX\prime}, \tag{4}$$

where the operators $\hat{p}^{ij}$ swap spins i and j. If the eigenvalue of $\hat{p}^{ij}$ is +1, the state is locally symmetric (for triplet states); if it is -1 the state is locally antisymmetric (for singlet states). If the eigenvalue of $\hat{p}_{global}$ is +1, the state is globally symmetric, which occurs when it is a product of an even number of antisymmetric singlet states, such as $T_0^{AA\prime}S_0^{MM\prime}S_0^{XX\prime}$. If the eigenvalue of $\hat{p}_{global}$ is -1 the state is globally antisymmetric with an odd number of singlet states, like $T_0^{AA\prime}T_0^{MM\prime}S_0^{XX\prime}$. All terms $\widehat{H}_Z$, $\widehat{H}_J^{geminal}$, $\widehat{H}_J^{vicinal}$, and $\widehat{H}_J^{long-range}$ commute with $\hat{p}_{global}$ since simultaneous permutation of the spins either leaves these terms unchanged or changes their sign.

Idealized Hamiltonian of the AA'MM'XX' spin system

Typically, the values of all geminal *J*-couplings $^2J_{HH}$ are similar in all CH_2 groups. Therefore, we may consider an *idealized Hamiltonian* that will allow us to develop an intuitive understanding of the spin dynamics.

(i) We assume that all geminal couplings in the aliphatic chain are equal:

$$J_{AA'} = J_{MM'} = J_{XX'} = J_{geminal} \tag{5}$$

(ii) We assume for simplicity that the vicinal couplings $^3J_{HH}$ obey the following equalities along the chain:

$$\begin{aligned} &J_{AM} = J_{A'M'} = J_{MX} = J_{M'X'}, \\ &J_{AM'} = J_{A'M} = J_{MX'} = J_{M'X}. \end{aligned} \tag{6}$$

so that the sums ΣJ and differences ΔJ are the same for all neighboring pairs of CH_2 groups along the entire aliphatic chain, i.e., $\Sigma J_{AM} = \Sigma J_{MX}$, and $\Delta J_{AM} = \Delta J_{MX}$. We define average parameters $\Sigma J = 1/2\,(\Sigma J_{AM} + \Sigma J_{MX})$ and $\Delta J = 1/2\,(\Delta J_{AM} + \Delta J_{MX})$.

(iii) Finally, we assume that all long-range couplings can be neglected:

$$J_{AX} = J_{A'X'} = J_{AX'} = J_{A'X'} = J_{long-range} = 0. \tag{7}$$

These assumptions amount to imposing a *translational symmetry*, so that the spin system of an aliphatic chain $(CH_2)_n$ has the characteristics of an ideal one-dimensional lattice with *n* nodes. Furthermore, we assume weak coupling between neighboring spin pairs, i.e., we assume that the difference in chemical shifts of neighboring CH_2 groups is much larger than the vicinal *J*-couplings. The idealized Hamiltonian is thus:

$$\begin{aligned} &\hat{H} = \hat{H}_Z + \hat{H}_J^{geminal} + \hat{H}_J^{vicinal}, \\ &\hat{H}_J^{geminal} = J_{geminal}\left(\hat{\boldsymbol{I}}^A \cdot \hat{\boldsymbol{I}}^{A'} + \hat{\boldsymbol{I}}^M \cdot \hat{\boldsymbol{I}}^{M'} + \hat{\boldsymbol{I}}^X \cdot \hat{\boldsymbol{I}}^{X'}\right), \\ &\hat{H}_J^{vicinal} = \tfrac{1}{2}\Sigma J\left[\left(\hat{I}_z^A + \hat{I}_z^{A'}\right)\left(\hat{I}_z^M + \hat{I}_z^{M'}\right) + \left(\hat{I}_z^M + \hat{I}_z^{M'}\right)\left(\hat{I}_z^X + \hat{I}_z^{X'}\right)\right] + \tfrac{1}{2}\Delta J\left[\left(\hat{I}_z^A - \right.\right. \\ &\left.\left.\hat{I}_z^{A'}\right)\left(\hat{I}_z^M - \hat{I}_z^{M'}\right) + \left(\hat{I}_z^M - \hat{I}_z^{M'}\right)\left(\hat{I}_z^X - \hat{I}_z^{X'}\right)\right] .. \end{aligned} \tag{8}$$

Only those terms which differ from Eq. (1) are given explicitly. The weak coupling approximation allows one to retain only longitudinal components like $\hat{I}_z^A$ of $\hat{H}_J^{vicinal}$ rather than the full vectors $\hat{\boldsymbol{I}}^A$. One may wonder to what extent the idealized Hamiltonian of Eq. (8) is realistic. The *J*-couplings of the AA'MM'XX' system of trimethylsilylpropanesulfonic acid (DSS) have been determined with great precision by exploiting the complementary information contained in ZQ and SQ spectra (**Table 1**). It appears that, by and large, the approximations of Eqs. (5)-(7) are reasonably well justified.

Table 1: Best estimates of the *J*-couplings of the AA'MM'XX' system of DSS, determined by complementary analysis of single- and zero-quantum spectra by iterative optimization of all the *J*-couplings with numerical diagonalization of the full Hamiltonian of Eq (1). The approximations of Eqs. (5) – (7) are justified to a reasonable extent.

Geminal couplings	Value (Hz)	Vicinal couplings	Value (Hz)	Long-range couplings	Value (Hz)
$J_{AA'}$	-14.03	$J_{AM} = J_{A'M'}$	10.58	$J_{AX} = J_{A'X'}$	-0.24
$J_{MM'}$	-13.53	$J_{A'M} = J_{AM'}$	5.26	$J_{AX'} = J_{A'X}$	-0.25
$J_{XX'}$	-14.24	$J_{MX} = J_{M'X'}$	11.77		
		$J_{M'X} = J_{MX'}$	5.22		
$\langle J_{geminal} \rangle$	-14	$\langle \Delta J \rangle$	6	$J_{long-range}$	0

Full singlet-triplet product basis

A system with 2n = 6 spins with I = 1/2 spans a Hilbert space with 2^6 = 64 spin states. A *full* singlet-triplet product basis can be constructed by taking all 4x4x4 = 64 direct products of the intra-pair singlet states $S_0^{KK'}$ and intra-pair triplet states $T_p^{KK'}$ with *p* = -1, 0, +1 and *KK'* = *AA'* or *MM'* or *XX'*:

$$\mathcal{B}_{loc}^{full} = \{S_0^{AA'}, T_{+1}^{AA'}, T_0^{AA'}, T_{-1}^{AA'}\} \otimes \{S_0^{MM'}, T_{+1}^{MM'}, T_0^{MM'}, T_{-1}^{MM'}\} \otimes \{S_0^{XX'}, T_{+1}^{XX'}, T_0^{XX'}, T_{-1}^{XX'}\}. \quad (9)$$

The resulting states, such as $S_0^{AA'} S_0^{MM'} S_0^{XX'}$ etc., will be referred to as *localized states* since they are represented by a product of eigenstates associated with individual spin pairs. These states can be separated into two distinct manifolds, 36 globally symmetric states and 28 globally antisymmetric states, comprising even and odd numbers of singlet states $S_0^{KK'}$, respectively. Their conventional ordering according to symmetry and total z-projection is given in Appendix I. The symmetric and antisymmetric manifolds are completely disconnected from each other: in the matrix representation of the full Hamiltonian of Eq. (1), there are no off-diagonal elements that connect the two manifolds, so that coherent evolution in these manifolds is completely independent.

Reduced singlet-triplet product basis

We choose to focus our attention on the manifold of states which can support collective long-lived zero-quantum coherences that can be experimentally excited and reconverted into observable magnetization by poly-SLIC sequences (see Methods). For this purpose, we only need to retain a *reduced* set of 2^3 = 8 states by excluding all triplet states $T_{+p}^{KK'}$ with $p \neq 0$:

$$\mathcal{B}_{loc}^{reduced} = \{S_0^{AA'}, T_0^{AA'}\} \otimes \{S_0^{MM'}, T_0^{MM'}\} \otimes \{S_0^{XX'}, T_0^{XX'}\}. \tag{10}$$

As a consequence of this reduction (**Fig. 1**, bottom), one neglects the 64-8 = 56 states involving terms $T_{+1}^{KK'}$ and $T_{-1}^{KK'}$. This implies that one ignores all ZQ transitions between pairs of spins that are *not* chemically equivalent, e.g., involving pairs like A and M, or M and X, which are exploited in conventional ZQ spectroscopy [34–39]. Of the 8 states of the reduced manifold $\mathcal{B}_{loc}^{reduced}$, 4 belong to the symmetric manifold $\mathcal{B}_{loc}^{sym}$. These will be numbered as follows:

$$\begin{aligned}
|1\rangle &= |S_0^{AA'} S_0^{MM'} T_0^{XX'}\rangle = |S_0 S_0 T_0\rangle, \\
|2\rangle &= |S_0^{AA'} T_0^{MM'} S_0^{XX'}\rangle = |S_0 T_0 S_0\rangle, \\
|3\rangle &= |T_0^{AA'} S_0^{MM'} S_0^{XX'}\rangle = |T_0 S_0 S_0\rangle, \\
|4\rangle &= |T_0^{AA'} T_0^{MM'} T_0^{XX'}\rangle = |T_0 T_0 T_0\rangle .
\end{aligned} \tag{11}$$

On the right-hand side, we have dropped the indices *AA'*, *MM'*, and *XX'* since the sequence of states suffices to identify the three neighboring spin pairs. The remaining 4 states belong to the antisymmetric manifold $\mathcal{B}_{loc}^{anti}$ of the reduced set $\mathcal{B}_{loc}^{reduced}$, and will be numbered as follows:

$$\begin{aligned}
|5\rangle &= |T_0^{AA'} T_0^{MM'} S_0^{XX'}\rangle = |T_0 T_0 S_0\rangle, \\
|6\rangle &= |T_0^{AA'} S_0^{MM'} T_0^{XX'}\rangle = |T_0 S_0 T_0\rangle, \\
|7\rangle &= |S_0^{AA'} T_0^{MM'} T_0^{XX'}\rangle = |S_0 T_0 T_0\rangle, \\
|8\rangle &= |S_0^{AA'} S_0^{MM'} S_0^{XX'}\rangle = |S_0 S_0 S_0\rangle.
\end{aligned} \tag{12}$$

These 8 localized states can be collected in the form of a column vector Φ_{loc}.

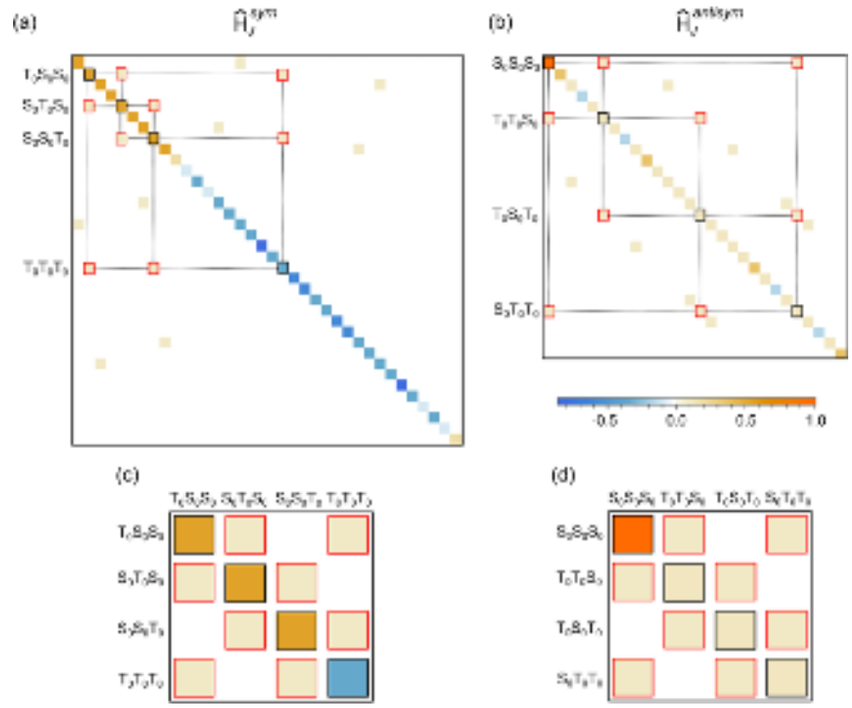

Fig. 1. (Top) Matrix representations of (a) the 36x36 globally symmetric and (b) the 28x28 antisymmetric manifolds of the idealized *J*-coupling Hamiltonian in the *full* singlet-triplet product basis $\mathcal{B}_{loc}^{full}$ of Eq. (9). The explicit ordering of the 64 states is given in the Appendix. (Bottom) Matrix representations of (c) the 4x4 globally symmetric and (d) the 4x4 antisymmetric manifolds of the Hamiltonian in the *reduced* singlet-triplet product basis $\mathcal{B}_{loc}^{reduced}$ of Eq (10). For $J_{geminal}$ = -14 Hz, ΔJ = 6 Hz, and ΣJ = 16 Hz, the elements are color-coded with -0.8 ≤ $\hat{H}_{ij}$ ≤ +1, normalized with respect to the antisymmetric diagonal element $\langle S_0S_0S_0|\hat{H}|S_0S_0S_0\rangle$ the-value of which is arbitrarily set to $\hat{H}_{ii}$ = +1.

Diagonalization of the idealized Hamiltonian in the reduced singlet-triplet product basis

In the limit where $\Delta J_{AM} = \Delta J_{MX} = \Delta J = 0$, we have a simple $A_2M_2X_2$ system with three geminal pairs of nuclei that are both chemically and magnetically equivalent. In this case, all 8 product states defined in Eq. (10-12) are good eigenstates. The energies of these states are shown in the upper part of **Fig. 2**. When $\Delta J = 0$, one cannot excite any LLSs or LLCs by SLIC. However, if $\Delta J \neq 0$, the geminal protons become magnetically inequivalent, so that off-diagonal elements appear in the matrix representation of the free precession Hamiltonian in the product basis (**Fig. 1**, top and bottom). Diagonalization of the Hamiltonian leads to mixing of the localized product states within both the symmetric and antisymmetric manifolds, resulting in a set of delocalized states.

A perturbation approach can be used to achieve a *partial* diagonalization of the idealized Hamiltonian because the couplings $J_{geminal}$ are much larger than the differences between the vicinal couplings ΔJ. The Hamiltonian can be split into two non-commuting parts, where the dominant term $\widehat{H}_0$ is given by:

$$\widehat{H}_0 = \widehat{H}_Z + J_{geminal}\left(\hat{\boldsymbol{I}}^A \cdot \hat{\boldsymbol{I}}^{A'} + \hat{\boldsymbol{I}}^M \cdot \hat{\boldsymbol{I}}^{M'} + \hat{\boldsymbol{I}}^X \cdot \hat{\boldsymbol{I}}^{X'}\right) + \frac{1}{2}\Sigma J\left[\left(\hat{I}_z^A + \hat{I}_z^{A'}\right)\left(\hat{I}_z^M + \hat{I}_z^{M'}\right) + \left(\hat{I}_z^M + \hat{I}_z^{M'}\right)\left(\hat{I}_z^X + \hat{I}_z^{X'}\right)\right]. \tag{13}$$

The remaining terms of the idealized Hamiltonian constitute a weak perturbation:

$$\widehat{H}_1 = \frac{1}{2}\Delta J\left(\hat{I}_z^A - \hat{I}_z^{A'}\right)\left(\hat{I}_z^M - \hat{I}_z^{M'}\right) + \frac{1}{2}\Delta J\left(\hat{I}_z^M - \hat{I}_z^{M'}\right)\left(\hat{I}_z^X - \hat{I}_z^{X'}\right). \tag{14}$$

The perturbation $\widehat{H}_1$ leads to off-diagonal elements in the $\mathcal{B}_{loc}^{reduced}$ basis. There exist analytical expressions to calculate matrix elements of the Zeeman and *J*-coupling terms of the spin Hamiltonian for arbitrarily large spin systems [40], page 159. Here we obtain an analytical form of the matrices by using the Spin Dynamica software [41], expressing the Hamiltonians in analytical form as in Eq. (13) and (14), choosing the basis $\mathcal{B}_{loc}^{full}$ and then calculating all the 16 matrix elements of $\widehat{H}_0$ and $\widehat{H}_1$ in the $\mathcal{B}_{loc}^{reduced}$ subspace. The matrix representations of $\widehat{H}_0 + \widehat{H}_1$ in the reduced basis $\mathcal{B}_{loc}^{reduced}$ are shown in **Fig. 1c** and **d**. Since the elements belonging to the states 1-8 are disconnected from all remaining states, as shown in **Fig. 1a** and **b** for the basis $\mathcal{B}_{loc}^{full}$, the perturbation analysis can be limited to the reduced set. For the symmetric manifold of Eqs. (11), two 4 x 4 matrices represent $\widehat{H}_0 + \widehat{H}_1$:

$$\left(\widehat{H}_0 + \widehat{H}_1\right)^{sym} = \frac{1}{4}J_{geminal}\begin{pmatrix} -5 & 0 & 0 & 0 \\ 0 & -5 & 0 & 0 \\ 0 & 0 & -5 & 0 \\ 0 & 0 & 0 & 3 \end{pmatrix} + \frac{1}{2}\Delta J\begin{pmatrix} 0 & 1 & 0 & 1 \\ 1 & 0 & 1 & 0 \\ 0 & 1 & 0 & 1 \\ 1 & 0 & 1 & 0 \end{pmatrix}, \tag{15}$$

Note that the terms proportional to ΣJ do not contribute to the Hamiltonian in this subspace. In the antisymmetric manifold of Eqs. (12), two similar 4 x 4 sub-matrices can be constructed for $\widehat{H}_0 + \widehat{H}_1$:

$$\left(\widehat{H}_0 + \widehat{H}_1\right)^{anti} = \frac{1}{4}J_{geminal}\begin{pmatrix} -1 & 0 & 0 & 0 \\ 0 & -1 & 0 & 0 \\ 0 & 0 & -1 & 0 \\ 0 & 0 & 0 & -9 \end{pmatrix} + \frac{1}{2}\Delta J\begin{pmatrix} 0 & 1 & 0 & 1 \\ 1 & 0 & 1 & 0 \\ 0 & 1 & 0 & 1 \\ 1 & 0 & 1 & 0 \end{pmatrix}, \tag{16}$$

If we consider only the Hamiltonian $\widehat{H}_0$, the three symmetric states $|1\rangle$, $|2\rangle$, and $|3\rangle$ are degenerate with energies $E(1) = E(2) = E(3) = -(5/4)\,J_{geminal}$, while level $|4\rangle$ has an energy of $E(4) = +(3/4)\,J_{geminal}$. Since geminal *J*-couplings of methylene groups are generally negative, the energies of the first three symmetric levels are higher than the energy of the fourth one, as shown in the bottom left of **Fig. 2**. The opposite applies to the antisymmetric states $|5\rangle$, $|6\rangle$, $|7\rangle$, and $|8\rangle$, as can be seen on the right-hand side of **Fig. 2**. In this case, the degenerate energies $E(4) = E(5) = E(6) = -(1/4)\,J_{geminal}$ are lower than $E(8) = -(9/4)\,J_{geminal}$. In both the symmetric and

antisymmetric manifolds, the energy difference between the three degenerate states and the fourth state is ΔE = $|2J_{geminal}|$. We shall only derive explicit expressions for the symmetric states $|1\rangle$, $|2$, $|3\rangle$, and $|4\rangle$, since similar derivations hold for the antisymmetric states.

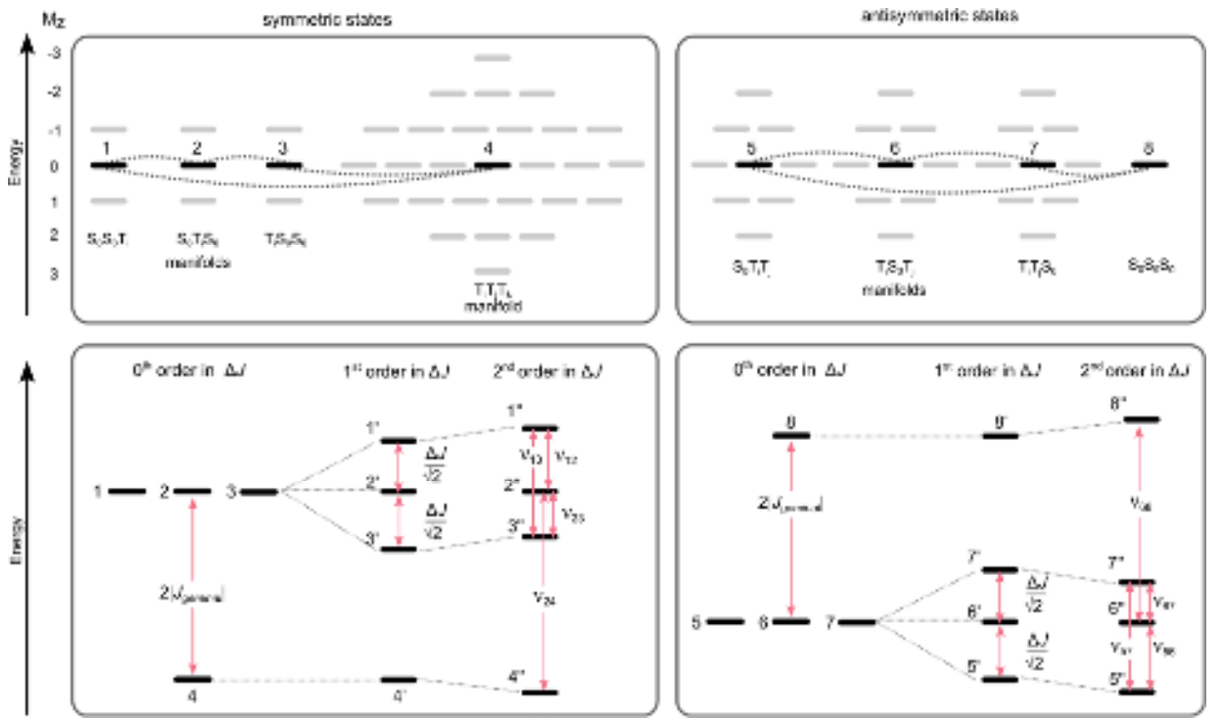

Fig. 2. (Top) Energy diagram of the full set $\mathcal{B}_{loc}^{full}$ of the 64 spin states of the AA'MM'XX' spin system in an external magnetic field, expressed in terms of products of singlet and triplet states. The numbers in the left margin show the z projections <M_z> of the total spin. Only levels shown in bold are connected by off-diagonal elements that are proportional to ΔJ, depicted by dotted lines. (Bottom) Expanded views of the energy-level diagrams of the reduced set $\mathcal{B}_{loc}^{reduced}$ of 2 x 4 = 8 states that are relevant for the ZQ spectra in this work. Diagonalization leads to mixing of these states. From left to right: zeroth, first- and second-order corrections in terms of ΔJ, assuming an idealized Hamiltonian with $J_{AA'} = J_{MM'} = J_{XX'} = J_{geminal}$, and $\Delta J_{AM} = \Delta J_{MX} = \Delta J \ll 2|J_{geminal}|$. (Left) States that are globally symmetric according to their symmetry with respect to three simultaneous intra-pair permutations. (Right) Globally antisymmetric states.

A partial diagonalization of the matrix representation of the Hamiltonian in both symmetric and antisymmetric blocks can be achieved by transformation into the following *delocalized* reduced basis:

$$(\hat{H})_{deloc} = U\,(\hat{H})_{loc}\,U^{-1}, \tag{17}$$

Where U and U^{-1} are unitary 4x4 matrices that transform the localized basis $\mathcal{B}_{loc}^{reduced}$ into the delocalized basis $\mathcal{B}_{deloc}^{reduced} = U\,\mathcal{B}_{loc}^{reduced}$:

$$U = U^{-1} = \frac{1}{2}\begin{pmatrix} 1 & \sqrt{2} & 1 & 0 \\ \sqrt{2} & 0 & -\sqrt{2} & 0 \\ 1 & -\sqrt{2} & 1 & 0 \\ 0 & 0 & 0 & 1 \end{pmatrix}. \tag{18}$$

Henceforth, we shall drop the labels "reduced" and "full". The explicit expression for the delocalized symmetrical states are:

$$\begin{aligned} |1'\rangle &= \tfrac{1}{2}\left(|S_0S_0T_0\rangle + \sqrt{2}|S_0T_0S_0\rangle + |T_0S_0S_0\rangle\right), \\ |2'\rangle &= \tfrac{1}{2}\left(\sqrt{2}|S_0S_0T_0\rangle - \sqrt{2}|T_0S_0S_0\rangle\right), \\ |3'\rangle &= \tfrac{1}{2}\left(|S_0S_0T_0\rangle - \sqrt{2}|S_0T_0S_0\rangle + |T_0S_0S_0\rangle\right), \\ |4'\rangle &= |4\rangle = |T_0T_0T_0\rangle. \end{aligned} \tag{19}$$

The matrix representation of the Hamiltonian in this new basis is:

$$\left(\hat{H}_0 + \hat{H}_1\right)^{sym}_{deloc} = \frac{J_{geminal}}{4}\begin{pmatrix} -5 & 0 & 0 & 0 \\ 0 & -5 & 0 & 0 \\ 0 & 0 & -5 & 0 \\ 0 & 0 & 0 & 3 \end{pmatrix} + \frac{\Delta J}{\sqrt{2}}\begin{pmatrix} 1 & 0 & 0 & 0 \\ 0 & 0 & 0 & 0 \\ 0 & 0 & -1 & 0 \\ 0 & 0 & 0 & 0 \end{pmatrix} + \frac{\Delta J}{2}\begin{pmatrix} 0 & 0 & 0 & 1 \\ 0 & 0 & 0 & 0 \\ 0 & 0 & 0 & 1 \\ 1 & 0 & 1 & 0 \end{pmatrix}, \tag{20}$$

The first two matrices are diagonal and provide first-order corrections to the energies:

$$\begin{aligned} E'(1) &= -(5/4)\, J_{geminal} + \left(1/\sqrt{2}\right)\Delta J, \\ E'(2) &= -(5/4)\, J_{geminal}, \\ E'(3) &= -(5/4) J_{geminal} - \left(1/\sqrt{2}\right)\Delta J, \\ E'(4) &= (3/4)\, J_{geminal}. \end{aligned} \tag{21}$$

At this point, the three states $|1'\rangle$, $|2'\rangle$, and $|3'\rangle$ are no longer degenerate but equidistant from each other as shown in the bottom left-hand side of **Fig. 2**, with the indication "correction to first-order in ΔJ". The third matrix in Eq. (20) contains off-diagonal elements between the "outer" states $|1'\rangle$ and $|3'\rangle$ and the "remote" state $|4'\rangle$. These off-diagonal elements are much smaller than the differences between the corresponding diagonal elements of the Hamiltonian, but they cannot be neglected for the qualitative description of experimental ZQ spectra. According to degenerate perturbation theory [42], the eigen-energies corrected to second-order are:

$$\begin{aligned} E''(1') &= -\tfrac{5}{4}\, J_{geminal} + \tfrac{1}{\sqrt{2}}\Delta J - \tfrac{1}{8}\frac{\Delta J^2}{J_{geminal}}, \\ E''(2') &= -\tfrac{5}{4}\, J_{geminal}, \end{aligned} \tag{22}$$

$$E''(3') = -\frac{5}{4}J_{geminal} - \frac{1}{\sqrt{2}}\Delta J - \frac{1}{8}\frac{\Delta J^2}{J_{geminal}},$$

$$E''(4') = \frac{3}{4}J_{geminal} + \frac{1}{8}\frac{\Delta J^2}{J_{geminal}},$$

as shown in the bottom right-hand side of **Fig. 2**, with the indication "correction to second order in ΔJ". The outer levels $|1'\rangle$ and $|3'\rangle$ now appear to be "repelled" with respect to the remote level $|4'\rangle$ so that they are no longer equidistant from the middle level $|2'\rangle$. The true eigenstates of the free precession Hamiltonian are only slightly different from the delocalized basis $\mathcal{B}_{deloc}$ of Eqs. (19). If we switch from the idealized Hamiltonian of Eq. (8) to the full Hamiltonian of Eq. (1), the eigen-energies can only be determined by numerical diagonalization, but the resulting exact eigenstates $\mathcal{B}_{eigen}$ of the full Hamiltonian remain to a very good approximation very similar to the delocalized basis $\mathcal{B}_{deloc}$, so that we can write:

$$\mathcal{B}_{deloc} \approx \mathcal{B}_{eigen}. \tag{23}$$

The approximate equality of Eq. (23) is consistent with the coefficients of the localized product states obtained by numerical diagonalization of the full Hamiltonian (see Appendix). Note that the energy $E''(4')$ is corrected to second order in ΔJ but the diagonalization does not significantly affect the eigenfunctions. We noticed in our experiments that ZQ coherences involving levels $|4'\rangle$ and $|8'\rangle$ are effectively destroyed by the filters used in the pulse sequence. Therefore, from now on, we will restrict the Hilbert space to the three delocalized states $|1'\rangle$, $|2'\rangle$, and $|3'\rangle$ in the symmetric manifold, and likewise to the states $|5'\rangle$, $|6'\rangle$, and $|7'\rangle$ in the antisymmetric manifold, ignoring the states $|4'\rangle$ and $|8'\rangle$.

Pairwise degenerate zero-quantum frequencies

The zero-quantum transition frequencies correspond to differences of the eigen-energies of Eq. (20) of the idealized Hamiltonian:

$$\begin{aligned} \nu_{12} &= E(1'') - E(2'') = \frac{1}{\sqrt{2}}\Delta J - \frac{1}{8}\frac{\Delta J^2}{J_{geminal}}, \\ \nu_{23} &= E(2'') - E(3'') = \frac{1}{\sqrt{2}}\Delta J + \frac{1}{8}\frac{\Delta J^2}{J_{geminal}}, \\ \nu_{13} &= E(1'') - E(3'') = \sqrt{2}\Delta J. \end{aligned} \tag{24}$$

The ZQ transitions are depicted by pink arrows in **Fig. 2b**. Although the approximations of Eqs. (5)-(7) are generally not quite accurate, the frequencies obtained in Eq. (24) are in reasonable agreement with the experimentally observed ZQ frequencies. Fortunately, the differences between geminal *J*-couplings can be determined with

sufficient precision from conventional 1D spectra, while differences ΔJ_{AM} and ΔJ_{MX} between vicinal *J*-couplings can be determined much more precisely from ZQ frequencies. A proper diagonalization of the full Hamiltonian using our best estimates of all couplings can only be carried out numerically. In a separate work, we have shown how one can iteratively analyze conventional 1D spectra and ZQ spectra to obtain precise values for geminal, vicinal and long-range *J*-couplings.

In the antisymmetric manifold, the same perturbative approach can be applied, leading to the following equalities:

$$\nu_{56} = \nu_{12}\,, \quad \nu_{67} = \nu_{23}\,, \quad \nu_{57} = \nu_{13}. \tag{25}$$

These equalities imply that each of the three signals in the ZQ spectrum results from an *exact superposition* of two distinct signals, one from the symmetric, the other from the antisymmetric manifold. This also holds if the full Hamiltonian of Eq. (1) is considered, without assuming an idealized spin system (Eq. (8)), i.e., without assuming all three geminal and the differences between vicinal coupling to be equal. Note that the *amplitudes* of these pairwise degenerate signals depend on the excitation and reconversion methods. As can be seen from **Table 3** in the Appendix, the amplitudes of the coherences between the antisymmetric states that are excited by various SLIC sequences are generally weaker than the amplitudes of the coherences between the symmetric states.

Projection operators

To visualize the behavior of the time-dependence of the states, which cannot be observed directly, in the evolution interval t_1, the density operator $\hat{\sigma}(t_1)$ can be *projected* onto one or several basis states $\hat{P}_k$. Formally, this can be written as:

$$\langle \hat{P}_k \rangle(t_1) = Tr\{\hat{P}_k \cdot \hat{\sigma}(t_1)\}. \tag{26}$$

In this work, we shall consider projections onto one of the 6 *localized* singlet-triplet product states $|k\rangle$ defined in Eqs. (11) and (12):

$$\hat{P}_k = |k\rangle\langle k| \text{ (with } k = 1, 2, 3 \text{ or } 5, 6, 7, \text{ but not } 4 \text{ and } 8) \tag{27}$$

Thus, for example $\hat{P}_{k=1} = |1\rangle\langle 1| = |S_0S_0T_0\rangle\langle S_0S_0T_0|$ extracts the part of the density operator that is proportional to the population of the localized state $|S_0S_0T_0\rangle$. We shall see below that suitable SLIC pulses can be used to materialize such mathematical projectors experimentally. The expectation values $\langle \hat{P}_k \rangle(t_1)$ can have positive or

negative values with respect to the average population of the triplet manifold $\overline{\sum_{\iota,J,k}|T_\iota T_J T_k\rangle\langle T_\iota T_J T_k|}$, which is manifested by an increase or decrease of the signal intensity after SLIC reconversion.

Irreducible tensor operators for the subspaces

Matrix representations of the irreducible tensor operators of three-level systems can be useful to describe the excitation and evolution of the ZQ coherences in the symmetric 3x3 subspaces in both Hilbert bases $\mathcal{B}_{loc}$and $\mathcal{B}_{deloc}$, as shown in **Fig. 3**. Similar matrices (not shown) can be defined for the antisymmetric 3x3 subspaces.

We can interpret the meaning of these matrices by referring to the energy-level diagram in **Fig. 2**. Let us first focus on the symmetrical states $|1'\rangle$, $|2'\rangle$ and $|3'\rangle$. Numerical simulations with the full Hamiltonian of Eq. (1) show that the coherences between levels $|1'\rangle \leftrightarrow |2'\rangle$ and $|2'\rangle \leftrightarrow |3'\rangle$ are always excited with approximately equal coefficients. Therefore, we construct operators and their matrix representations which describe these coherences together. The $\hat{A}_x$ operator, when it is represented in the basis $\mathcal{B}_{loc}$ (second column of **Fig. 3**) corresponds to a population imbalance between the symmetric states $|1\rangle\langle 1| = |S_0S_0T_0\rangle\langle S_0S_0T_0|$ and $|3\rangle\langle 3| = |T_0S_0S_0\rangle\langle T_0S_0S_0|$. On the other hand, when the same operator $\hat{A}_x$ is represented in the basis $\mathcal{B}_{deloc}$ (third column of **Fig. 3**), it describes a superposition of two ZQ coherences $|1'\rangle\langle 2'| + |2'\rangle\langle 1'|$ and $|2'\rangle\langle 3'| + |3'\rangle\langle 2'|$. Both of these coherences have real amplitudes, described by the phase "x". This state can be also represented by the sum of two single-transition operators $\hat{I}_x^{1',2'} + \hat{I}_x^{2',3'}$.

Similarly, $\hat{A}_y$ describes the case in which the same two ZQ coherences have phase "y". We can therefore say that the operators $\hat{A}_x$ and $\hat{A}_y$ describe an *in-phase* superposition of two ZQCs ($\hat{A}_x \propto |1'\rangle\langle 2'| + |2'\rangle\langle 1'| + |2'\rangle\langle 3'| + |3'\rangle\langle 2'|, \hat{A}_y \propto i|1'\rangle\langle 2'| - i|2'\rangle\langle 1'| + i|2'\rangle\langle 3'| - i|3'\rangle\langle 2'|$). Analogously, operators $\hat{B}_x$ and $\hat{B}_y$ represent an *anti-phase* superposition of the same two ZQCs ($\hat{B}_x \propto |1'\rangle\langle 2'| + |2'\rangle\langle 1'| - |2'\rangle\langle 3'| - |3'\rangle\langle 2'|$, $\hat{B}_y \propto i|1'\rangle\langle 2'| - i|2'\rangle\langle 1'| - i|2'\rangle\langle 3'| + i|3'\rangle\langle 2'|$). The operators $\hat{C}_x$ and $\hat{C}_y$ are used to describe the coherence in the two-level system spanned by the states $|1'\rangle$ and $|3'\rangle$. These are reminiscent of double-quantum transitions in a spin I = 1. In addition to these six operators, we employ the operators $\hat{T}_{10}$ and $\hat{T}_{20}$ to describe the population differences between the states $|1'\rangle$, $|2'\rangle$ and $|3'\rangle$. If the populations of all three states are equal, this is described by $\hat{T}_{00}$. These 9 operators form a complete Liouville basis of the subspace and allow us to describe any states in the reduced basis that can be excited by SLIC excitation schemes (see Appendix).

	$\mathcal{B}_{loc}$	$\mathcal{B}_{deloc}$	Tensors
T_{00}	$\frac{1}{\sqrt{3}}\begin{pmatrix}1&0&0\\0&1&0\\0&0&1\end{pmatrix}$	$\frac{1}{\sqrt{3}}\begin{pmatrix}1&0&0\\0&1&0\\0&0&1\end{pmatrix}$	$\frac{1}{\sqrt{3}}T_{00}$
T_{10}	$\frac{1}{2}\begin{pmatrix}0&1&0\\1&0&1\\0&1&0\end{pmatrix}$	$\frac{1}{\sqrt{2}}\begin{pmatrix}1&0&0\\0&0&0\\0&0&-1\end{pmatrix}$	$\frac{1}{\sqrt{2}}T_{10}$
T_{20}	$\frac{1}{2\sqrt{6}}\begin{pmatrix}-1&0&3\\0&2&0\\3&0&-1\end{pmatrix}$	$\frac{1}{\sqrt{6}}\begin{pmatrix}1&0&0\\0&-2&0\\0&0&1\end{pmatrix}$	T_{20}
A_x	$\frac{1}{\sqrt{2}}\begin{pmatrix}1&0&0\\0&0&0\\0&0&-1\end{pmatrix}$	$\frac{1}{2}\begin{pmatrix}0&1&0\\1&0&1\\0&1&0\end{pmatrix}$	$\frac{1}{2}(T_{1-1}-T_{11})$
A_y	$\frac{i}{2}\begin{pmatrix}0&1&0\\-1&0&1\\0&-1&0\end{pmatrix}$	$\frac{i}{2}\begin{pmatrix}0&-1&0\\1&0&-1\\0&1&0\end{pmatrix}$	$\frac{i}{2}(T_{1-1}+T_{11})$
B_x	$\frac{1}{2}\begin{pmatrix}0&1&0\\1&0&-1\\0&-1&0\end{pmatrix}$	$\frac{1}{2}\begin{pmatrix}0&1&0\\1&0&-1\\0&-1&0\end{pmatrix}$	$\frac{1}{\sqrt{2}}(T_{2-1}-T_{21})$
B_y	$\frac{i}{\sqrt{2}}\begin{pmatrix}0&0&1\\0&0&0\\-1&0&0\end{pmatrix}$	$\frac{i}{2}\begin{pmatrix}0&-1&0\\1&0&1\\0&-1&0\end{pmatrix}$	$\frac{1}{\sqrt{2}}(T_{2-1}+T_{21})$
C_x	$\frac{1}{2\sqrt{2}}\begin{pmatrix}1&0&1\\0&-2&0\\1&0&1\end{pmatrix}$	$\frac{1}{\sqrt{2}}\begin{pmatrix}0&0&1\\0&0&0\\1&0&0\end{pmatrix}$	$\frac{1}{\sqrt{2}}(T_{2-2}+T_{22})$
C_y	$\frac{i}{2}\begin{pmatrix}0&1&0\\-1&0&-1\\0&1&0\end{pmatrix}$	$\frac{i}{\sqrt{2}}\begin{pmatrix}0&0&-1\\0&0&0\\1&0&0\end{pmatrix}$	$\frac{1}{\sqrt{2}}(T_{2-2}-T_{22})$

Fig. 3. Matrix representations of an orthonormal basis set of operators in 3x3 subspaces that can be used to describe populations and coherences between the three levels $|1'\rangle, |2'\rangle, |3'\rangle$ in the localized product basis $\mathcal{B}_{loc}$ (left), in the delocalized basis $\mathcal{B}_{deloc}$ (middle), and in terms of irreducible tensor operators of a three-level system (right) . A similar set can be defined for the three levels $|5'\rangle, |6'\rangle, |7'\rangle$ **.** The interconversion of the matrices between localized and delocalized bases can be achieved by $M' = U\,M\,U^{-1}$, where U is defined in Eq. (18). All matrices are normalized to fulfill $\sqrt{Tr(M^T M)} = 1$.

It can be shown that only four terms – two LLS-related terms ($\hat{T}_{10}$ and $\hat{T}_{20}$) and two LLC-related terms ($\hat{A}_x$ and $\hat{C}_x$) – can be excited and reconverted from observable magnetization and back using SLIC pulses. None of the 9 remaining operators in Fig. 3 can be reconverted, so that they can be considered as "silent" or "unobservable".

Invariant and oscillating components of the density operator

The spin dynamics in each reduced 3x3 subspace can be described by evolution of a *state vector* in Liouville space. Both the state vector $\hat{\sigma}$ and the full scalar coupling Hamiltonian $\hat{H}_J$ of Eq (1) (or the idealized form of Eq.(8)) can be represented as vectors in this Liouville space. If these vectors are parallel, their commutator will vanish:

$$\left[\hat{\sigma}^{parallel}, \hat{H}_J\right] = 0, \tag{28}$$

so that there will be no evolution, apart from relaxation. One may speak of invariants of motion [43]. A component $\hat{\sigma}_r^{parallel}$ that is parallel to the vector H_J corresponds to a long-lived state. Various excitation methods using single- or double-SLIC also allow one to excite states that generally do *not* commute with the Hamiltonian in the subspace:

$$\left[\hat{\sigma}_r^{orthogonal}, \hat{H}_J\right] \neq 0. \tag{29}$$

Such components will precess in a plane perpendicular to the vector $\hat{H}_J$ at a frequency given by the strength of $\hat{H}_J$:

$$\hat{\sigma}_r^{orthogonal}(t_1) = \hat{\sigma}_r^{orthogonal}(0) exp(-i\,\omega_r t_1) \sum_s C_{rs} exp(-t_1/T_{LLC}^s). \tag{30}$$

Thus, a component that is orthogonal to the vector H_J corresponds to a (possibly long-lived) ZQ coherence. Barring degeneracies, their magnitudes usually decay mono-exponentially, so that there is again only one non-vanishing coefficient $C_{rr} = 1$.

In actual fact, the ZQCs are pairwise degenerate, with pairs of terms belonging to the symmetric and antisymmetric manifolds. These terms could in principle have different lifetimes T_{LLC}^s. Thus, states like $|S_0S_0T_0\rangle$ and $|S_0T_0T_0\rangle$ are likely to have different lifetimes, bearing in mind that $T_1^{A} = T_1^{A'}$ can be different from $T_1^{X} = T_1^{X'}$. Off-diagonal terms in the matrix of coefficients (C_{rs}) represent couplings that may be not negligible between degenerate coherences [44]. However, If the relaxation (super-) operator does not contain any elements that violate the global permutation symmetry, all couplings C_{rs} between degenerate coherences must be zero. Note that this may not be applicable when a ligand that carries an LLS or LLC binds to a chiral protein.

Free precession of ZQ coherences

The density operator spanned by the symmetrical states $|1\rangle$, $|2\rangle$, $|3\rangle$ in the eigenbasis of the free precession Hamiltonian can be split into LLS and LLC parts:

$$\hat{\sigma}_{LLS} = \lambda_1\hat{T}_{00} + \lambda_2\hat{T}_{10} + \lambda_3\hat{T}_{20} \tag{31}$$

$$\hat{\sigma}_{LLC} = \lambda_4(t)\hat{A}_x + \lambda_5(t)\,\hat{A}_y + \lambda_6(t)\,\hat{B}_x + \lambda_7(t)\,\hat{B}_y + \lambda_8(t)\,\hat{C}_x + \lambda_9(t)\,\hat{C}_y.$$

Where the density operator $\hat{\sigma}_{LLS}$ describes the populations in the 3x3 subspace while $\hat{\sigma}_{LLC}$ describes the ZQ coherences in this same subspace. Similar expressions apply for the antisymmetric states $|5\rangle$,$|6\rangle$, $|7\rangle$). Assuming that at time t = 0, only in-phase terms are present in the density operator, the coefficients of the 9 operator terms have the following time dependence:

$$\lambda_4(t) = \lambda_4(0)\tfrac{1}{2}(cos[2\pi\nu_{12}t] + cos[2\pi\nu_{23}t]), \tag{32}$$

$$\lambda_5(t) = \lambda_4(0)\tfrac{1}{2}(sin[2\pi\nu_{12}t] + sin[2\pi\nu_{23}t]),$$

$$\lambda_6(t) = \lambda_4(0)\tfrac{1}{2}(sin[2\pi\nu_{12}t] - sin[2\pi\nu_{23}t]),$$

$$\lambda_7(t) = \lambda_4(0)\tfrac{1}{2}(cos[2\pi\nu_{23}t] - cos[2\pi\nu_{12}t]).$$

These 4 equations describe the evolution of the density operator terms $\hat{A}_x$, $\hat{A}_y$, $\hat{B}_x$, and $\hat{B}_y$ (**Fig. 3**). Out of these four terms, only $\hat{A}_x$ is "reconvertable" into observable magnetization by SLIC, so that the signal will be modulated by the two frequencies ν_{12} and ν_{23} contained in $\lambda_4(t)$.

Furthermore, the precession in the two-dimensional subspace spanned by the operators $\hat{C}_x$ and $\hat{C}_y$ leads to

$$\lambda_8(t) = \lambda_8(0)cos[2\pi(\nu_{13})t] \tag{33}$$

$$\lambda_9(t) = \lambda_8(0)sin[2\pi(\nu_{13})t],$$

Note that the subspace spanned by the operators $\hat{T}_{10}$, $\hat{C}_x$ and $\hat{C}_y$ can be represented on a Bloch sphere by noticing that the matrix representations of these three operators in the delocalized basis coincides with the three Pauli matrices for a spin ½, unlike the operators $\hat{A}_x$, $\hat{A}_y$, $\hat{B}_x$, and $\hat{B}_y$. Since only the term $\hat{C}_x$ is reconvertable into observable magnetization by SLIC, the signal will be modulated at the frequency ν_{13} contained in $\lambda_8(t)$

Methods

A generic pulse sequence that is suitable to excite both LLSs and LLCs and that can probe their evolution and relaxation is shown in **Fig. 4**. This sequence is similar to the ones used in our earlier work [16] and is inspired by the pioneering work of DeVience et al. [22]. In our earlier work [16], some LLCs were excited along with LLSs but they were not discussed in any detail. The first SLIC irradiation populates various singlet-triplet product states in the molecule of interest, which then evolve and relax during the t_1 evolution period. After applying a T_{00} filter, they are reconverted into observable magnetization by a SLIC pulse, so that an NMR signal can be detected during the t_2 period. The experiments presented here use polychromatic SLIC (poly-SLIC) pulses [16] to unequally populate various singlet-triplet product states like $|S_0S_0T_0\rangle\langle S_0S_0T_0|$, $|S_0T_0S_0\rangle\langle S_0T_0S_0|$, and $|T_0S_0S_0\rangle\langle T_0S_0S_0|$. There are several poly-SLIC pulses which can be used for this purpose, two of which are shown by way of examples in **Fig. 4b** and **c.** These and other methods are represented by pictograms drawn on the molecular structures in panel **g**. In all cases, the excitation starts by applying a 'hard' non-selective $90°_x$ pulse. This can be replaced by one, two or three simultaneous selective $90°_x$ pulses. In this work, the initial excitation is followed by double SLIC irradiation that is selectively applied

at the chemical shifts $\nu_A = \nu_{A'}$ and/or $\nu_M = \nu_{M'}$ and/or $\nu_X = \nu_{X'}$ of the three proton pairs. The RF amplitude can be chosen to fulfill the "single quantum" (SQ) condition of the level anti-crossings (LACs) responsible for the excitation. For SQ-SLIC pulses, the optimum amplitude and duration are [45]:

$$\nu_1^{SQ-SLIC} = \left|2J_{geminal}\right|, \qquad \tau_{SQ-SLIC} = 1/\left(\sqrt{2}\cdot \Delta J\right). \tag{34}$$

The optimum duration of SQ-SLIC pulses is determined by the requirement that the populations of two levels must be swapped (in analogy to the effect of a 180° pulse on an isolated spin $I = ½$). Alternatively, one can choose a weaker RF amplitude to fulfill the "double quantum" (DQ) condition of the LACs. This requires only half the RF amplitude, but the optimum duration must be extended by a factor $\sqrt{2}$:

$$\nu_1^{DQ-SLIC} = \left|J_{geminal}\right|, \qquad \tau_{DQ-SLIC} = 1/(\Delta J). \tag{35}$$

In practice, one can optimize the RF amplitude and the duration of the SLIC pulses empirically. This allows one to estimate average values of $J_{geminal}$ (usually in the vicinity of $J_{geminal}$= -14 Hz in aliphatic CH_2 groups) and ΔJ which may span a range $0 < \Delta J < 6$ Hz, depending on the populations of the rotamers [45].

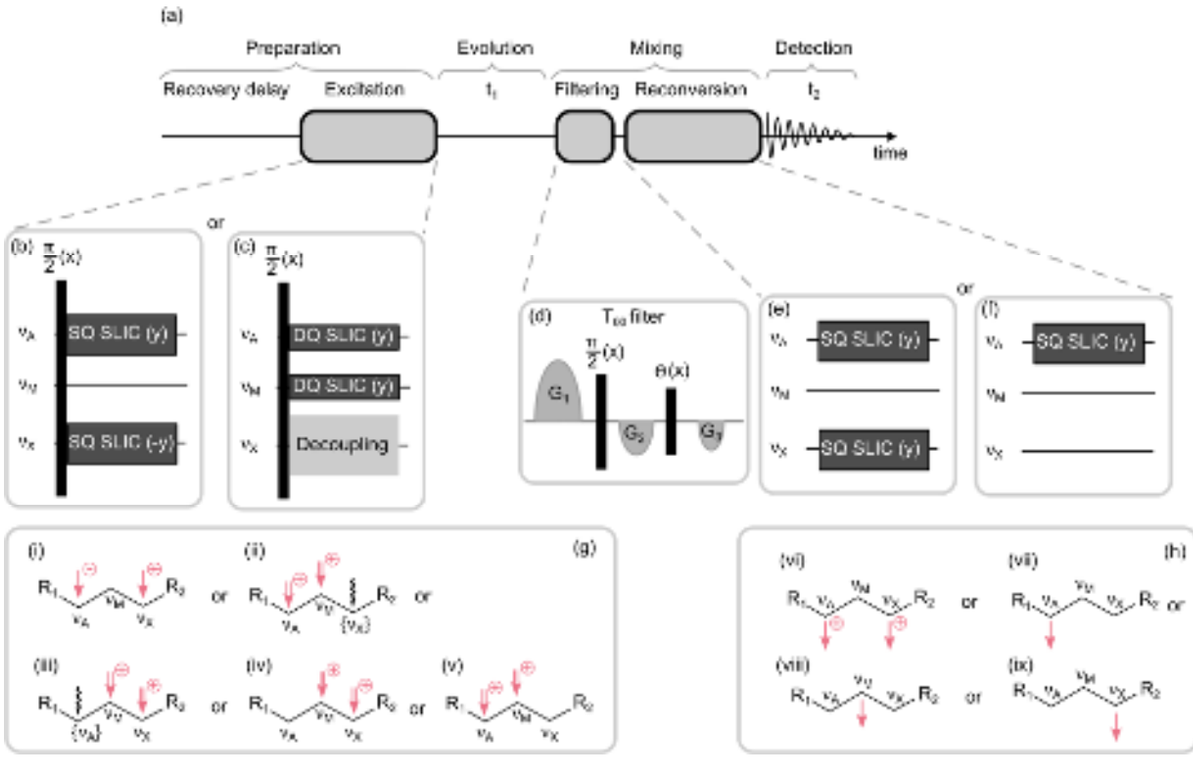

Fig. 4. Pulse sequences used in this work. (a) General scheme with a recovery delay, the excitation of LLSs and LLCs by one of several possible poly-SLIC schemes with or without decoupling, t_1 evolution, T_{00} filtering, reconversion into observable magnetization by further poly-SLIC pulses, and finally a detection period t_2. Phase-cycling selects the coherence order p = 0 to retain both populations and zero-quantum coherences (ZQCs) in the t_1 interval [46]. (b) Antiphase-SQ-AX-SLIC excitation with RF phases +y and -y. (c) In-phase-DQ-AM-SLIC{X}, where spins X and X' are decoupled during SLIC excitation, which is represented by {X}. (d) A T_{00}-filter [47] is applied in the manner of Sabba et al. [48], where the π/2 pulse can be replaced by a composite pulse of the type BB1 [49]. (e) and (f) Examples of double- and single-SLIC pulses that can be used to reconvert LLSs and LLCs into observable magnetization. (g) Examples of possible excitation schemes displayed as pictograms. The pink arrows *above* the molecular structures indicate the RF fields applied to CH_2 groups for the excitation. The +/- signs in pink circles denote the relative phases of the two SLIC pulses. The wavy black arrows indicate the CH_2 groups that are decoupled during excitation. (h) Similar pictogram representations of some possible reconversion schemes using single- and double-SLIC, indicated by arrows shown *below* the molecular structures.

Fig. 4b shows a novel variant of the poly-SLIC excitation scheme where, after the initial 90° pulse, two RF fields with equal amplitudes $\nu_1^{SQ-SLIC}$ but with *opposite initial phases* are applied simultaneously at the chemical shifts $\nu_A = \nu_{A'}$ and $\nu_X = \nu_{X'}$. We term this excitation scheme *antiphase-SQ-AX-SLIC.* The Hamiltonians that describe these two RF fields in a doubly-rotating frame can be written as:

$$H_{RF}^{anti-SQ-SLIC} = \nu_1^{SQ-SLIC}\left(\hat{I}_y^A + \hat{I}_y^{A'}\right) + k\,\nu_1^{SQ-SLIC}\left(\hat{I}_y^X + \hat{I}_y^{X'}\right), \tag{36}$$

Where k = -1 for *antiphase-SQ-AX-SLIC*, as shown in **Fig. 4b**, which is in contrast to *in-phase-SQ-AX-SLIC* used for reconversion with k = +1 (**Fig. 4e**).

An alternative excitation that maximizes the non-uniformity of the amplitudes of the relevant singlet-triplet-product states is the *in-phase-DQ-AM-SLIC{X}* method shown in **Fig. 4c**. Two RF fields with the *same* initial phase are applied simultaneously at the chemical shifts ν_A and ν_M. At the same time, the X and X' spins are *decoupled,* which is represented by the usual symbo*l {X}*. This has the effect of tailoring the length of the aliphatic chain during the excitation and allows one to confine the excited terms to the two CH_2 groups of the A, A' and M, M' spins. The Hamiltonian in a triply-rotating frame during *in-phase-DQ-AM-SLIC{X}* excitation with decoupling of XX' is:

$$H_{RF}^{DQ-SLIC(AM)\{X\}} = \nu_1^{DQ-SLIC}\left(\hat{I}_y^A + \hat{I}_y^{A\prime}\right) + \nu_1^{DQ-SLIC}\left(\hat{I}_y^M + \hat{I}_y^{M\prime}\right) + \nu_1^{dec}\left(\hat{I}_y^X + \hat{I}_y^{X\prime}\right), \tag{37}$$

where ν_1^{dec} stands for the RF amplitude of the decoupling field, which should be larger than $\left|J_{geminal}\right|$ and ΔJ, but smaller than the differences between the chemical shifts $|\nu_A - \nu_X|$ and $|\nu_M - \nu_X|$. Typically, we use ν_1^{dec} = 100 Hz if the chemical shifts are not too close. Bloch-Siegert shifts [50] may have to be taken into account. The phase of the decoupling field is immaterial.

A third possibility to excite LLCs is *in-phase*-DQ-SLIC applied at the chemical shifts ν_A and ν_M *without* decoupling of X and X' (*in-phase-DQ-AM-SLIC*). In this case, the efficiency of the excitation is roughly 66 % of what can be achieved with decoupling, but this can still be a method of choice if the chemical shifts are too close to perform proper decoupling or to achieve efficient *antiphase-SQ-AX-SLIC* excitation. The conversion efficiencies of all these methods are recapitulated in the Appendix (**Table 3**). **Fig. 4e**, **f** and **g** show different options for the reconversion SLIC pulses. We use a self-explanatory graphical representation to specify at which chemical shifts the SLIC pulses are applied (**Fig. 4g** and **h**).

Results and discussion

The action of the SLIC pulse leads to the over- or underpopulation of symmetrical states $|1\rangle$, $|2\rangle$, and $|3\rangle$ with respect to the average population $\overline{\left|T_i T_j T_k\right\rangle\left\langle T_i T_j T_k\right|}$. A similar effect occurs for the antisymmetrical states $|5\rangle$, $|6\rangle$, $|7\rangle$ with respect to the unique state $|S_0 S_0 S_0\rangle$. **Fig. 5** introduces a graphical representation of these population imbalances. For example, a population imbalance between $|3\rangle = |S_0 S_0 T_0\rangle$ and the mean population of the 27 triplet states $\left|T_i T_j T_k\right\rangle$ is depicted graphically by two blue circles on a schematic molecular structure (**Fig. 5**, upper left). These blue circles are filled or empty for positive or negative imbalances. Population imbalances involving any of the remaining

states are depicted according to the same principle. All of these population imbalances are "reconvertable" since the application of a reconversion SLIC pulse can transform them back into observable magnetization.

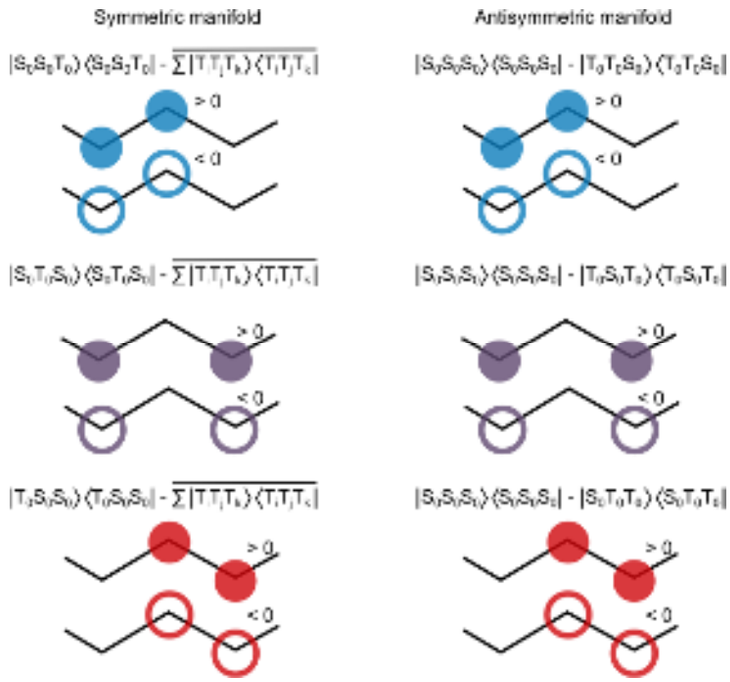

Fig. 5. Graphical representation of singlet-triplet population imbalances associated with spins AA' and MM' are depicted in blue, those associated with AA' and XX' in purple, those associated with MM' and XX' in red. Filled and empty circles represent population imbalances with positive and negative signs.

The excited density operator depends on the SLIC irradiation scheme. For example, *anti-phase*-SQ-AX-SLIC irradiation leads to an overpopulation of $|1\rangle = |T_0S_0S_0\rangle$ and $|5\rangle = |T_0T_0S_0\rangle$ and a simultaneous underpopulation of $|3\rangle = |S_0S_0T_0\rangle$ and $|7\rangle = |S_0T_0T_0\rangle$, which corresponds to $\hat{A}_x$ (**Fig. 3**) in both symmetric and antisymmetric manifolds of $\mathcal{B}_{loc}$ and $\mathcal{B}_{deloc}$:

$$\left(\hat{\sigma}_{antiphase-SLIC(AX)}\right)_{loc} = \frac{1}{\sqrt{2}}\begin{pmatrix}1 & 0 & 0\\ 0 & 0 & 0\\ 0 & 0 & -1\end{pmatrix}, \tag{38}$$

$$\left(\hat{\sigma}_{antiphase-SLIC(AX)}\right)_{deloc} = \frac{1}{2}\begin{pmatrix}0 & 1 & 0\\ 1 & 0 & 1\\ 0 & 1 & 0\end{pmatrix}. \tag{39}$$

When using the *in-phase*-DQ-AM-SLIC excitation scheme – be it with or without decoupling of X and X' during SLIC – the resulting population imbalance in the symmetric subsystem can be written as the follows:

$$\left(\hat{\sigma}_{in-phase-SLIC(AM)}\right)_{loc} = \frac{1}{\sqrt{2}}\begin{pmatrix}2 & 0 & 0\\ 0 & 0 & 0\\ 0 & 0 & 0\end{pmatrix} = \frac{1}{\sqrt{2}}\begin{pmatrix}1 & 0 & 0\\ 0 & 0 & 0\\ 0 & 0 & -1\end{pmatrix} + \frac{1}{\sqrt{2}}\begin{pmatrix}1 & 0 & 0\\ 0 & 0 & 0\\ 0 & 0 & 1\end{pmatrix}. \tag{40}$$

The first term on the right-hand side is the same as the operator $\hat{A}_x$ in eq. (38). The last term represents a population imbalance between $|2\rangle = |S_0T_0S_0\rangle$ and the two equally populated states $|1\rangle = |T_0S_0S_0\rangle$ and $|3\rangle = |S_0S_0T_0\rangle$. In the basis $\mathcal{B}_{deloc}$ this corresponds to:

$$\left(\hat{\sigma}_{in-phase-SLIC(AM)}\right)_{deloc} = \frac{1}{2\sqrt{2}}\begin{pmatrix}1 & 0 & 1\\ 0 & 2 & 0\\ 1 & 0 & 1\end{pmatrix}. \tag{41}$$

This expression describes an imbalance between the population of $|2'\rangle$ and the two equal populations of the "outer" states $|1'\rangle$ and $|3'\rangle$, plus a zero-quantum coherence $\hat{C}_x = \hat{I}_x^{(1',3')}$ between levels $|1'\rangle$ and $|3'\rangle$. The expressions for ZQ coherences shown here are supported by numerical simulations (see Appendix.)

Non-adiabatic interconversion

The $\hat{A}_x$ operator corresponds to a population imbalance when represented in the basis $\mathcal{B}_{loc}$ and at the same time describes ZQ coherences in the basis $\mathcal{B}_{deloc}$. In the absence of RF irradiation, i.e., in the evolution period t_1, the relevant basis is the eigenbasis of the free precession Hamiltonian [51]. In the presence of RF fields, i.e., during excitation or reconversion by polychromatic SLIC irradiation, the relevant basis is the eigenbasis in the doubly- (or multiply-) rotating frame. Thus "population imbalances" in the rotating frame may be converted instantaneously (i.e., non-adiabatically) into collective LLCs in the laboratory frame when the RF fields are switched off at the beginning of the evolution interval t_1. These coherences are then reconverted into population imbalances in the rotating frame when the RF fields are switched back on after the T_{00} filter. A similar approach involving a change of basis (using the 'Zeeman basis' during the excitation and the 'singlet-triplet basis' during the sustaining period) was proposed by Vasos *et al*. [10] to gain an understanding of the spin dynamics for the unique LLC in a system with two spins with $I = ½$.

Projections and reconversion by SLIC

One can project the density operator $\hat{\sigma}(t_1)_{filtered}$ (i.e., at the end of the evolution interval t_1, after the T_{00} filter and the phase cycle) onto one or several terms of the *localized* basis. In this work we are interested in the projections onto one of the three localized symmetrical states $|S_0S_0T_0\rangle$, $|S_0T_0S_0\rangle$, or $|T_0S_0S_0\rangle$, or one of the three localized anti-symmetrical states $|S_0T_0T_0\rangle$, $|T_0S_0T_0\rangle$, or $|T_0T_0S_0\rangle$. However, such a formal projection operation does not provide a prescription for experimental measurements.

One of the central tenets of this paper is that the oscillating signal observed after the action of the superoperator $\hat{\hat{P}}_{SLIC}$ that describes the reconversion into single-quantum coherences in the subsequent detection interval t_2 is proportional to the expectation value of P_k:

$$\langle s(t_1)\rangle = Tr\left\{\hat{I}_x, \hat{\hat{P}}_{SLIC}\,\hat{\sigma}(t_1)_{filtered}\right\}. \tag{42}$$

The details of the reconversion process are complex, since they involve dynamics occurring at LACs conditions that depend on the number of selective RF fields (single- or double SLIC), their relative phases (in-phase or antiphase), their RF amplitudes (to match the SQ or DQ conditions), and their durations τ_{SLIC}. Furthermore, our unitary numerical simulations based on SpinDynamica [41] do not account for relaxation phenomena during the reconversion process, with rates of the type $1/T_{1rho}$ that depend on many parameters.

Fortunately, the equivalence between Eqs. (26) and (42) can be shown heuristically. **Fig. 6** shows dynamics of expectation values calculated using Eq. (26) by projecting $\hat{\sigma}(t_1)_{filtered}$ onto two of the *localized* states $|S_0S_0T_0\rangle\langle S_0S_0T_0|$ (blue) and $|T_0S_0S_0\rangle\langle T_0S_0S_0|$ (red), using our best estimates of the scalar couplings of the full Hamiltonian of DSS (**Table 1**), after the T_{00} filter that is applied at the end of the evolution interval t_1, assuming that the excitation prior to t_1 was achieved either by *anti-phase*-SQ-AX-SLIC or *in-phase*-DQ-MX-SLIC{A}.

Although we cannot provide a rigorous proof at this time, one obtains very similar results experimentally by reconversion of $\hat{\sigma}(t_1)_{filtered}$ into $\langle s(t_1)\rangle$ according to Eq.(42) when $\hat{P}_{SLIC}$ is materialized by *in-phase*-SQ-AX-SLIC. Indeed, **Fig. 7** shows comparisons of the *experimental* signals observed at the chemical shifts of XX' (dark red) and AA' (dark blue) with the *simulated* expectation values of $|S_0S_0T_0\rangle\langle S_0S_0T_0|$ (light blue) and $|T_0S_0S_0\rangle\langle T_0S_0S_0|$ (light red), both reproduced from **Fig. 6**. Thus *in-phase*-SQ-AX-SLIC offers an effective means of converting into observable magnetization the two localized terms $|S_0S_0T_0\rangle\langle S_0S_0T_0|$ and $|T_0S_0S_0\rangle\langle T_0S_0S_0|$ that are represented by blue and red lines in **Fig. 6** at the end of the evolution interval t_1.

Propagation of spin order

As we have seen, the spin dynamics during free evolution can be considered in different bases. In the *delocalized* eigenbasis of free precession, the ZQ coherences are represented by off-diagonal matrix elements and precess in the course of time. Their characteristic frequency is determined by the difference between the energies of the eigenstates that they span. However, we can also project $\hat{\sigma}(t_1)_{filtered}$ onto states of the *localized* product basis, which is not an eigenbasis during free evolution. This has the advantage that one can associate the over-/under-populations of localized states in $\mathcal{B}_{loc}$ of different spin pairs in the molecule and superimpose a schematic representation of singlet-triplet product states onto the molecular structure.

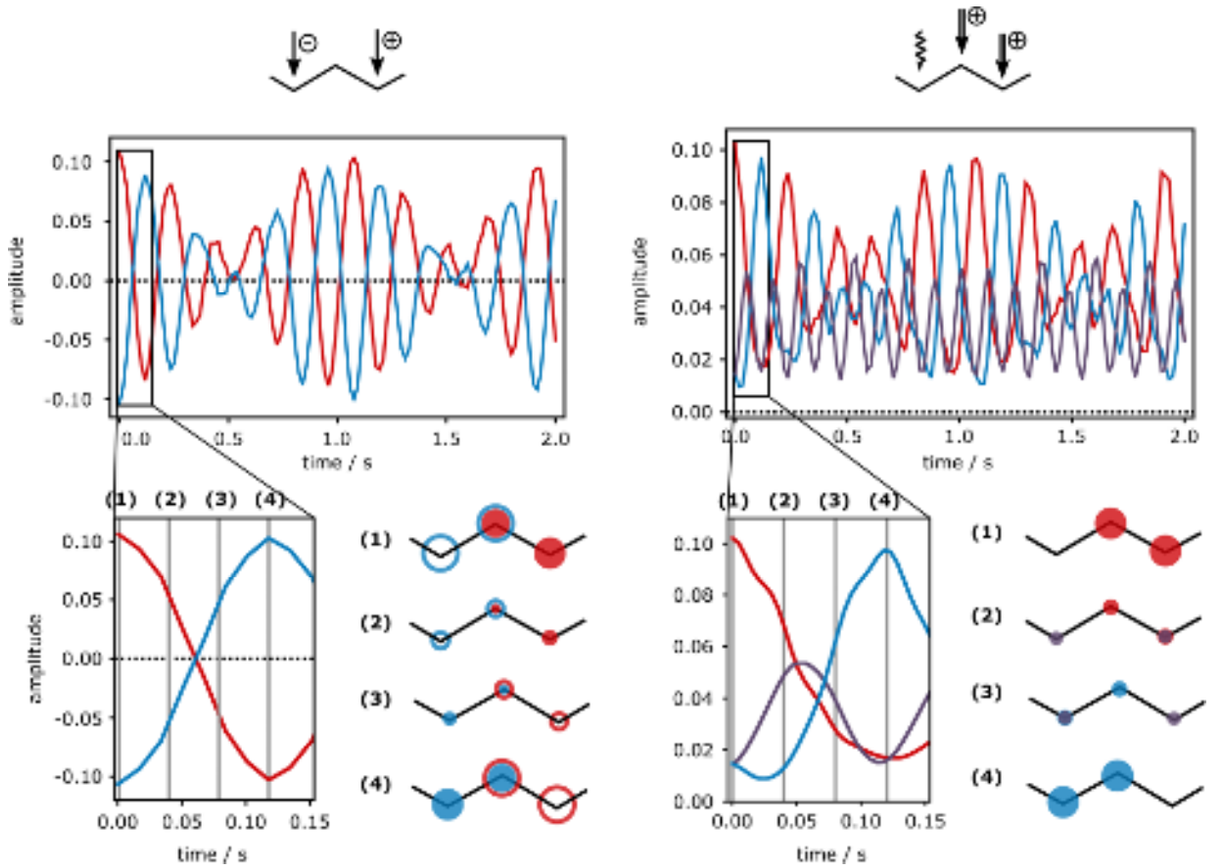

Fig. 6. (Top) Simulated expectation values of the populations of localized states $|T_0S_0S_0\rangle$ (red) and $|S_0S_0T_0\rangle$ (blue) over the course of the evolution time t_1 after excitation using (left) *anti-phase*-SQ-AX-SLIC or (right) *in-phase*-DQ-MX-SLIC{A}. (Bottom) Expanded views of the first 150 ms of the simulated t_1 oscillations. Different time points in the trajectories are marked by numbers **(1)**-**(4)**. For each of these points, graphical representations of the amplitudes of the states $|T_0S_0S_0\rangle$, $|S_0T_0S_0\rangle$, $|S_0S_0T_0\rangle$ are superimposed on a schematic drawing of the molecule DSS. The open and filled circles indicate whether the expectation values are positive or negative.

Such graphical representations at four different time points marked **(1)** to **(4)** are shown on the left-hand side of **Fig. 6**: **(1)** At t = 0, immediately after *anti-phase*-SQ-AX-SLIC excitation, there is an underpopulation of the state $|S_0S_0T_0\rangle$ (depicted by empty blue circles) and a simultaneous overpopulation of the state $|T_0S_0S_0\rangle$ (depicted by filled red circles). **(2)** As time evolves, the coefficient of $|S_0S_0T_0\rangle$ increases, while the coefficient of $|T_0S_0S_0\rangle$ decreases, so that **(3)** at $t \approx 0.075$ ms, the signs of both terms change, and **(4)** at $t \approx 0.12$ ms, the situation is reversed with respect to **(1)**, resulting in a positive term $|S_0S_0T_0\rangle$ and a negative term $|T_0S_0S_0\rangle$. A similar effect is shown on the right-hand side of **Fig. 6** for *in-phase*-DQ-MX-SLIC{A} excitation. Note that the imbalances do not change sign in this case. These figures illustrate how spin order propagates, moving back and forth along a chain of finite length, like a particle in a box. While this is unusual for free precession, similar phenomena have been observed under RF irradiation [27,28,30].

By projecting the density operator onto one of the *localized* states $|k\rangle$ defined in Eqs. (11) and (12) (with k = 1, 2, 3 or 5, 6, 7, but not 4 and 8), one sees that the oscillating part of the observable magnetization after reconversion is, to a good approximation, proportional to the over-/under-populations of the localized states. This is apparent when comparing experimental signals $s(t_1)$ and simulated coefficients of these localized states. **Fig. 7** shows the time dependence of the integrals of the multiplets of AA' (dark blue) and XX' (dark red) in the molecule DSS where the ZQ coherences are excited by *anti-phase*-SQ-AX-SLIC or *in-phase*-DQ-MX-SLIC{A} with decoupling of A and A'. No Fourier transformation was carried out with respect to t_1. Simulations of the populations of the states $|T_0S_0S_0\rangle$ and $|S_0S_0T_0\rangle$ were carried out using our best estimates of the *J*-couplings of **Table 1** rather than those of the idealized Hamiltonian. These oscillations correspond very closely to the observed oscillations of experimental signals, except for some minor high-frequency modulations due to transitions that we neglected.

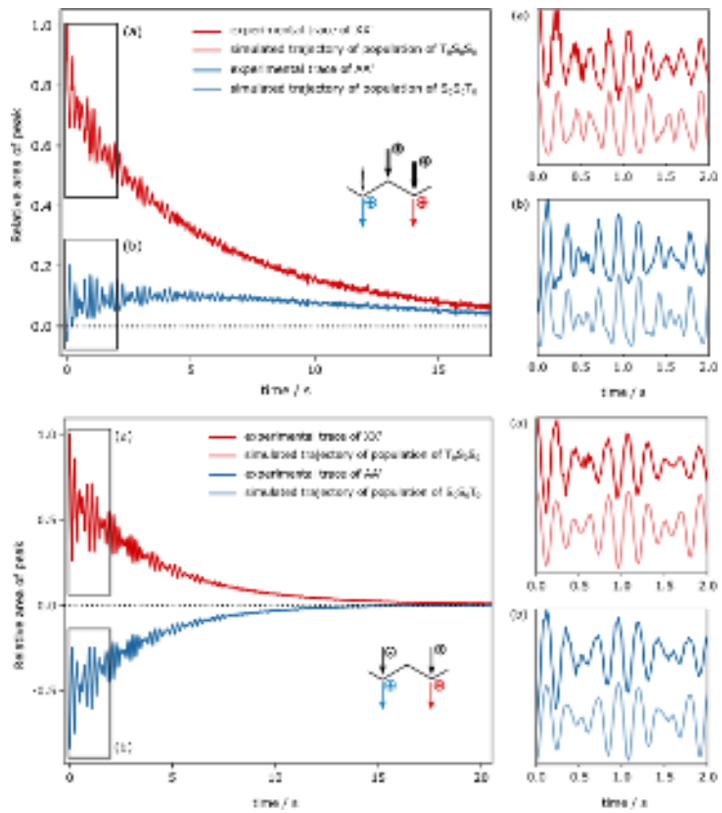

Fig. 7: (Top left) Experimental signals of trimethylsilylpropanesulfonic acid (DSS) recorded as a function of the evolution time t_1 after *in-phase*-DQ-MX-SLIC{A} excitation and *in-phase*-SQ-AX-SLIC reconversion. (Bottom left) Integrals of DSS multiplets recorded in the detection interval t_2 as a function of the evolution time t_1 after *anti-phase*-SQ-AX-SLIC excitation and *in-phase*-SQ-AX-SLIC reconversion. (Right) Experimental signals (dark

colors) of XX' (red) and AA' (blue) compared with simulated expectation values (light colors) of localized $|T_0S_0S_0\rangle$ (red) and $|S_0S_0T_0\rangle$ (blue) states. The best estimates of the *J*-couplings used for the simulations are shown in **Table 1**.

The populations of the states $|1\rangle$, $|2\rangle$, and $|3\rangle$ are proportional to the coherences described by operators $\hat{A}_x$ and $\hat{C}_x$. In the case of *antiphase*-SQ-AX-SLIC excitation in **Fig. 7** (bottom), no ZQ coherences of the type described by $\hat{C}_x$ are excited. The $\hat{A}_x$ operator, however, is excited efficiently. Since this operator comprises two distinct ZQ coherences, it evolves with two distinct frequencies. As these frequencies are close to one another, this leads to a low frequency beating. The oscillations are superimposed onto an unmodulated, slowly decaying component, which is due to the LLS.

In the case of *in-phase*-DQ-MX-SLIC{A} excitation (**Fig. 7**, top), the three ZQ coherences described by both $\hat{A}_x$ and $\hat{C}_x$ are excited. Thus, the time evolution of the experimental signals contains three distinct frequencies. It is interesting to note that the unmodulated component of the trace belonging to the AA' spin pair has a vanishing initial amplitude, as opposed to the negative values obtained when using *anti-phase*-SQ-AX-SLIC excitation.

When carefully comparing the experimental traces with the simulated populations, one can see that the experimental signals contain some high-frequency oscillations that do not appear in the simulations. These oscillations are due to the ZQ coherence between levels $|2'\rangle$ and $|4'\rangle$ in the symmetric manifold, and to the coherence between levels $|6'\rangle$ and $|8'\rangle$ in the antisymmetric manifold in **Fig. 2**. It seems that – in contrast to the simulations – these coherences are not fully suppressed in experiments by the T_{00} filter. This could be due to pulse imperfections.

Experimental zero-quantum (ZQ) spectra

ZQ spectra were obtained by performing a complex Fourier transformation of the single-quantum signals detected in the t_2-dimension and a real (cosine) transformation of the oscillations observed indirectly in the t_1-dimension, which leads to pure 2D absorption-absorption lineshapes. An example of a 2D spectrum of DSS using *in-phase*-DQ-AM-SLIC excitation and *anti-phase*-SQ-AX-SLIC reconversion is shown in **Fig. 8** (top). There are three ZQ peaks in ω_1 at the chemical shifts of AA' and XX' in the ω_2 dimension.

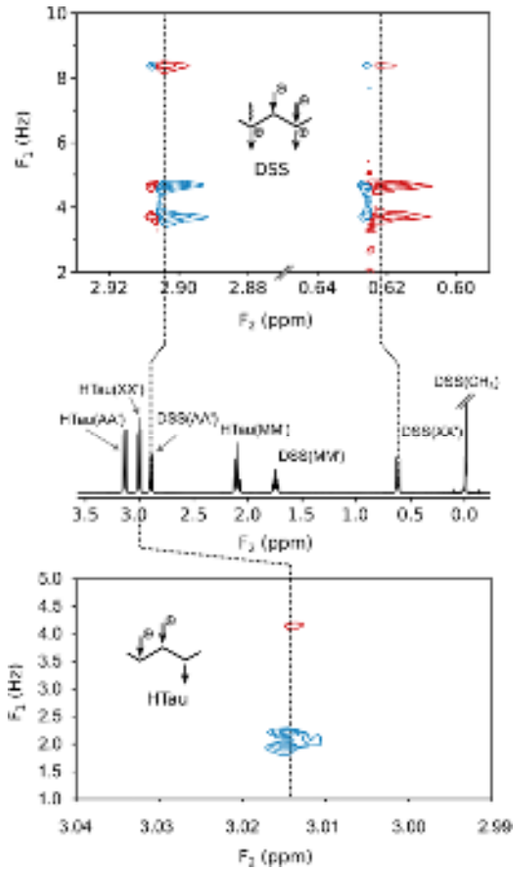

Fig. 8. (Middle) Conventional ^{1}H spectrum with signal assignments of a sample containing a mixture of ca. 50 mM trimethylsilylpropanesulfonic acid (DSS) and ca. 50 mM homotaurine (HTau) in D_2O. The chemical shifts of AA' and XX' of DSS are indicated by dotted lines. (Top) Expanded view of a 2D ZQ spectrum of DSS using *in-phase*-DQ-MX-SLIC{A} excitation while decoupling the AA' pair, combined with *in-phase*-SQ-AX-SLIC reconversion. (Bottom) Expanded view of a ZQ spectrum of HTau using *in-phase*-DQ-AM-SLIC excitation without decoupling, followed by SQ-X-SLIC reconversion.

Fig. 9a shows cross-sections along ω_1 of the same 2D spectrum of DSS at the chemical shifts in ω_2 of AA' (red spectrum) and XX' (blue signals). The frequencies of the ZQ peaks in the ω_1-dimension are labelled ν_{ij}, where *i* and *j* refer to delocalized eigenstates. In **Fig. 9a**, the two peaks at $\nu_{12} = 4.67$ Hz and $\nu_{23} = 3.70$ Hz have approximately equal intensities, showing that these ZQ coherences are excited equally. The linewidths of these peaks are on the order of 120 mHz. The peak at $\nu_{13} = 8.37$ Hz has a lower intensity and appears at the same frequency as the $\nu_{12} + \nu_{23} = 8.37$ Hz, which agrees with the energy level structure shown in **Fig. 2**. The peak associated with the coherence 2'-4' appears at $\nu_{24} = 26.9$ Hz and has a nearly negligible amplitude. **Fig. 9c** shows the ZQ spectrum for DSS excited with *anti-phase*-SQ-AX-SLIC and selective decoupling applied to XX' during the evolution interval t_1. Decoupling during free evolution has the effect of effectively "shortening" the chain of coupled methylene groups from *n* = 3 to *n* = 2. Thus, selective decoupling of XX' during the evolution interval t_1 leads in effect to reduce the 6-spin system to a mere 4-spin system, which entails a simplification of both Hilbert space and eigenbasis of the Hamiltonian, causing the 3-level system in **Fig. 2** to collapse into a 2-level system. These two levels correspond to the states $|T_0^{AA'}S_0^{MM'}\rangle$ and $|S_0^{AA'}T_0^{MM'}\rangle$, whose energies differ by ΔJ_{AM} [17]. The two states can only support a single ZQ coherence, and indeed,

the experimental ZQ spectrum contains a single dominant signal at 5.45 Hz ≈ ΔJ_{AM} = 5.32 Hz. The origin of the weak signals around 2 and 3 Hz is the subject of further investigation but may be related to the imperfect selectivity of the decoupling. Note that the intensity of the peak at υ_{24} (blue trace) appears to be enhanced when observed on the AA' multiplet. In a complementary experiment (not shown), selective decoupling was applied to the AA' spins during t_1. In the resulting spectrum, the peak with the highest intensity has a frequency of 6.63 Hz, which approximately matches ΔJ_{MX} = 6.55 Hz (**Table 1**). The discrepancy of ca. 0.1 Hz of determined values of ΔJ_{AM} and ΔJ_{MX} obtained from the experiments with and without selective decoupling during t_1 will be the subject of further research. Perhaps it can be explained either by imperfections of the selective decoupling or by local minima of the complementary analysis of 1D and ZQ spectra.

Similar ZQ spectra were also acquired for HTau (**Fig. 9b**, **d**). The ZQ coherences were excited using *in-phase*-DQ-AM-SLIC and reconverted into magnetization using either SQ-A-SLIC (**Fig. 9b**) or SQ-X-SLIC (**Fig. 9d**). In these spectra, three peaks appear at $\nu_{23} = 1.97$ Hz, $\nu_{12} = 2.20$ Hz, and $\nu_{13} = 4.15$ Hz $\approx \nu_{12} + \nu_{23} = 4.17$ Hz.

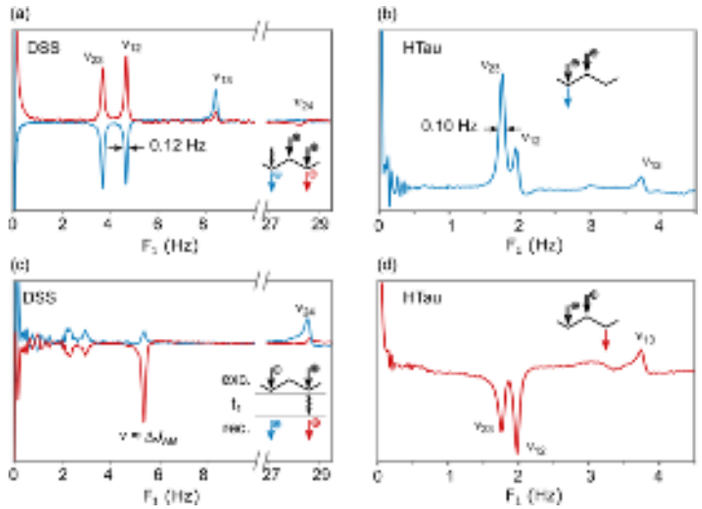

Fig. 9. Cross-sections parallel to the ω_1 axis of ZQ spectra of DSS (left) and homotaurine (right). Figures (a) and (c) show cross-sections at the ω_2 frequencies of the chemical shifts of AA' (red trace) and XX' (blue trace). The coherences were excited using either (a) *in-phase*-DQ-MX{A} or (c) *anti-phase*-SQ-AX-SLIC and reconverted in both (a) and (c) using *in-phase*-SQ-AX-SLIC. In the case of (c), selective decoupling was applied at the chemical shifts of XX' during the evolution interval t_1, leading in effect to a reduction of the AA'MM'XX' system to a mere AA'MM' system in t_1. In the ZQ spectrum, this leads to a collapse of the peaks at the frequencies ν_{23}, ν_{12} and ν_{13} and to a unique peak at a frequency of *ca.* ΔJ_{AM}, as discussed in the text. Both ZQ spectra of homotaurine in (b) and (d) were obtained with *in-phase*-DQ-AM-SLIC for excitation, while the reconversion was achieved using either SQ-A-SLIC (b) or SQ-X-SLIC (d).

The linewidths of these ZQ spectra can be used to determine the lifetimes of the collective ZQ coherences as $T_{LLC} = 1/(\pi\Delta\nu)$ (where $\Delta\nu$ is the full width at half height). For DSS this gives a T_{LLC} of 2.7 s, whereas the T_2 of the aliphatic

protons found in the CPMG experiments was 1.7 s. For HTau $T_{LLC} = 3.2$ s, and the corresponding $T_2 = 2.3$ s. Therefore, we conclude that the collective coherences observed in the introduced experiments are long-lived.

Experimental

All NMR spectra were obtained at 298 K with a 5-mm iProbe in a Bruker 500 MHz WB magnet (B_0 = 11.66 T) equipped with a "Neo" console. The sample contained a mixture of *ca.* 50 mM of trimethylsilylpropanesulfonic acid (DSS) and *ca.* 50 mM Homotaurine (HTau) in D_2O and was not degassed.

The SLIC pulse sequences used are shown in **Fig. 4**. For DSS the SLIC pulses had an amplitude of ν_{SLIC} = 27 Hz and a duration of τ_{SLIC} = 110 ms (to match the SQ condition), or ν_{SLIC} = 14 Hz and τ_{SLIC} = 155 ms (for the DQ condition). The SLIC pulses used for HTau had an RF amplitude ν_{SLIC} = 26 Hz and a duration τ_{SLIC} = 180 ms (SQ condition) or ν_{SLIC} = 13 Hz and τ_{SLIC} = 254 ms (DQ condition). Multiple frequencies for poly-SLIC were generated by the superposition of rectangular phase-modulated pulses. To remove spin order of ranks $0 < l \leq 3$, a single-scan T_{00} filter was used, consisting of three G_z gradient pulses, each followed by a delay of 200 ms and interleaved with three non-selective 90° pulses. The latter can be replaced by composite pulses of the type BB1 [49]. The three gradients had sinusoidal shapes and durations of 4.4, 2.4, and 2.0 ms, while their amplitudes were set to 10, −10, and 15% of the maximum available field gradient G_z = 50 G/cm = 0.5 T/m. The first RF pulse of the T_{00} filter, applied between the first and second gradients, had a phase ϕ = 90° (i.e., along the y-axis), and the second and third pulses were applied after the second and third gradients, with phases ϕ = 54.7° and 0°, respectively. A four-step phase cycle was used in all experiments, by alternating the phases of the excitation SLIC pulses (y, −y, y, −y) and of the reconversion SLIC pulses (y, y, −y, −y), while the phase of the receiver followed the pattern (y, −y, −y, y). In principle, the recovery delays must exceed 5 T_{LLS}, unless one destroys all remaining LLS [52]. In this work, we have used recovery delays as short as 5 T_1, i.e., much shorter than 5 T_{LLS}. The ZQ spectrum of DSS obtained by exciting with *in-phase*-DQ-MX{A} was acquired with 4 transients, t_1^{max} = 17 s, and 1024 increments with Δt_1 = 16.666 ms. The ZQ spectrum of DSS excited with *anti-phase*-SQ-AX-SLIC and decoupling during t_1 was acquired with 4 transients, t_1^{max} = 20.48 s, and 1024 increments with Δt_1 = 20 ms. Both ZQ spectra of HTau were acquired with 8 transients, t_1^{max} = 20 s, and 400 increments with Δt_1 = 50 ms. In all cases, the t_1-dependent oscillating signals arising from the collective LLCs were transformed into the ω_1 frequency domain by a real (cosine) Fourier transformation.

Conclusions

The present work represents an extension of more familiar applications of zero-quantum spectroscopy, which exploit scalar couplings between chemically inequivalent spins [34–39]. In our work, the frequencies of the ZQ peaks can be determined experimentally with a precision on the order of 10 mHz, a feature that will be exploited in a forthcoming paper. We shall demonstrate how the comparison between ZQ spectra and conventional SQ spectra allows one to determine all scalar couplings of an AA'MM'XX' spin system with unprecedented accuracy. We shall exploit this ZQ spectroscopy to determine the energies of the potential wells of rotamers. Finally, we shall show that ZQ coherences are affected by binding to macromolecules such as proteins in view of drug screening. Even with a very low protein concentration, weak binding in the rapid exchange regime dramatically accelerates the relaxation rate constants R_{LLC}, or, equivalently, reduces the time constant T_{LLC}, and hence broadens the lines in ZQ spectra. This effect may be exacerbated for BSA which is known to have multiple non-selective binding sites. The contrast between free and bound ligands should be useful to improve drug screening methods. *Inter alia*, this is due to the fact that an achiral molecule that carries an LLS or LLC experiences a loss of symmetry when it forms a (transient) complex with a (chiral) protein. The contrast between free and bound molecules is exacerbated in experiments that are affected by a change of spin symmetry, rather than by a mere change of rotational diffusion times [53–55]. The development of LLS and LLC methods therefore offers a promising approach for fragment-based drug discovery (FBDD), where one seeks to identify fragments of potential drugs that have a rather weak affinity for their target, so that the exchange between free and bound drugs remains rapid on the time-scale of relaxation in the bound form [53,56]. These aspects will be discussed in more detail in a forthcoming paper. The ZQ methods can be used for the precise determination of vicinal *J*-couplings, and therefore to determine populations of rotamers by Karplus relations.

Here, we have demonstrated various methods to observe collective long-lived zero-quantum coherences in aliphatic chains. An analytical approach was developed to describe the spin dynamics, showing that the behavior of collective LLCs can be understood as a propagation of spin order along the chain of methylene protons. We like to refer to these ZQ experiments in aliphatic chains as *spin-chain ZQ spectroscopy*. In each CH_2 group, the pair of states S_0 and T_0 spans a two-level subsystem that can be described by a fictitious spin $I = ½$. A chain of such two-level subsystems bears analogies to one-dimensional chains of unpaired electron spins with $I = ½$. The length of the chain need not be restricted to the case of $n = 3$ considered here, so that novel experiments may be designed for longer aliphatic chains.

Acknowledgements

We are grateful to Philippe Pelupessy for useful discussions. We are indebted to the CNRS and the ENS for support, and to the European Research Council (ERC) for the Synergy grant "Highly Informative Drug Screening by Overcoming NMR Restrictions" (HISCORE, Grant Agreement No. 951459).

Appendix

A1. Singlet-triplet product basis

Order of states in the full singlet-triplet product basis used in the matrix representations of **Fig. 1**.

Symmetric block:

$T_+S_0S_0$, $T_0S_0S_0$, $T_-S_0S_0$, $S_0T_+S_0$, $S_0T_0S_0$, $S_0T_-S_0$, $S_0T_+S_0$, $S_0S_0T_+$, $S_0S_0T_0$, $S_0S_0T_-$, $T_+T_+T_+$, $T_0T_+T_+$, $T_+T_0T_+$, $T_+T_+T_0$, $T_0T_0T_+$, $T_0T_+T_0$, $T_+T_0T_0$, $T_-T_+T_+$, $T_+T_-T_+$, $T_+T_+T_-$, $T_0T_0T_0$, $T_-T_+T_0$, $T_+T_-T_0$, $T_+T_0T_-$, $T_-T_0T_+$, $T_0T_-T_+$, $T_0T_+T_-$, $T_0T_0T_-$, $T_0T_-T_0$, $T_-T_0T_0$, $T_-T_-T_+$, $T_-T_+T_-$, $T_+T_-T_-$, $T_0T_-T_-$, $T_-T_0T_-$, $T_-T_-T_0$, $T_-T_-T_-$.

Antisymmetric block:

$S_0S_0S_0$, $S_0T_+T_+$, $S_0T_0T_+$, $S_0T_-T_+$, $S_0T_+T_0$, $S_0T_0T_0$, $S_0T_-T_0$, $S_0T_+T_-$, $S_0T_0T_-$, $S_0T_-T_-$, $T_+S_0T_+$, $T_0S_0T_+$, $T_-S_0T_+$, $T_+S_0T_0$, $T_0S_0T_0$, $T_-S_0T_0$, $T_+S_0T_-$, $T_0S_0T_-$, $T_-S_0T_-$, $T_+T_+S_0$, $T_0T_+S_0$, $T_-T_+S_0$, $T_+T_0S_0$, $T_0T_0S_0$, $T_-T_0S_0$, $T_+T_-S_0$, $T_0T_-S_0$, $T_-T_-S_0$.

A2. Coefficients of true eigenstates expressed in terms of idealized states

The approximate equality of Eq. (23) can be justified by comparing the coefficients in **Table 2**.

Table 2. Scalar products $\langle\phi_p^{eigen}|\phi_q'\rangle$and $\langle\phi_p^{eigen}|\phi_q''\rangle$ taken between the true eigenstates $\phi_p^{eigen} \in \mathcal{B}^{eigen}$ found by numerical diagonalization of the (non-idealized) Hamiltonian of Eq. (1) for the case of DSS with our best estimates of the *J*-couplings. The singly-primed states $\phi_p' \in \mathcal{B}_{deloc}^{sym}$ were obtained from Eq.(17) derived by zeroth-order perturbation theory. The doubly-primed states $\phi_p'' \in \mathcal{B}''^{sym}_{deloc}$ of Eq. (A1) were derived by first-order perturbation theory. Note that coefficients in the vicinity of 0.99 (bold numbers) confirm that both singly- and doubly-primed states are good approximations of the true eigenstates.

	$\|1'\rangle$	$\|2'\rangle$	$\|3'\rangle$	$\|4'\rangle$	$\|1''\rangle$	$\|2''\rangle$	$\|3''\rangle$	$\|4''\rangle$
$\langle 1\|$	**0.9955**	0.0280	-0.0001	0.0907	**0.9988**	0.0280	0.0275	-0.0149
$\langle 2\|$	-0.0250	**0.9905**	0.1313	-0.0321	-0.0331	**0.9905**	0.1330	-0.0154
$\langle 3\|$	0.0145	-0.1339	**0.9840**	-0.1168	-0.0347	-0.1339	**0.9906**	-0.0136
$\langle 4\|$	-0.0904	0.0138	0.1204	**0.9881**	0.0100	0.0138	0.0120	**0.9992**

The doubly-primed states ϕ_p'' corresponded to functions calculated according to first-order degenerate perturbation theory for the eigenstates. They can be expressed in terms of the singly-primed states ϕ_p' as:

$$|1''\rangle = \frac{1}{\langle 1''|1''\rangle}\left(|1'\rangle - \frac{\Delta J}{4\,J_{geminal}}\left\{|4'\rangle + \frac{2}{\sqrt{2}}|3'\rangle\right\}\right), \tag{A1}$$

$$|2''\rangle = |2'\rangle,$$

$$|3''\rangle = \frac{1}{\langle 3''|3''\rangle}\left(|3'\rangle - \frac{\Delta J}{4\,J_{geminal}}\left\{|4'\rangle + \frac{2}{\sqrt{2}}|1'\rangle\right\}\right),$$

$$|4''\rangle = \frac{1}{\langle 4''|4''\rangle}\left(|4'\rangle + \frac{\Delta J}{4\,J_{geminal}}\{|1'\rangle + |3'\rangle\}\right).$$

A3. Numerical simulations of the excitation efficiency

The efficiency of the excitation of the individual terms depends on the SLIC scheme. **Table 3** below shows the coefficients for the terms described by the operators introduced in **Fig. 3**.

Table 3. Excitation efficiency for the symmetric and the antisymmetric manifolds after using different poly-SLIC schemes applied to DSS with the *J*-couplings specified in **Table 1**. Terms with coefficients below 0.04 in the symmetric subspace are deemed negligible and are not shown. The coefficients are calculated by projecting the simulated density operator $\hat{\sigma}$ onto one of the irreducible tensor operators $\hat{T}_{lp}$ (see **Fig. 3**) according to $Tr\left\{\left(\frac{\hat{\sigma}}{\|\hat{\sigma}\|}\right)^T\left(\frac{\hat{T}_{lp}}{\|\hat{T}_{lp}\|}\right)\right\}$.

Irradiation scheme	*Anti-phase*-double *SQ-AX-SLIC*	*In-phase*-double *DQ-AM-SLIC*	*In-phase*-double *DQ-AM-SLIC {X}* *with decoupling of XX'*
Symmetric subspace			
λ_1 ($\hat{T}_{00}$)	0	-0.19	-0.26
λ_3 ($\hat{T}_{20}$)	0	0.06	0.09
λ_4 ($\hat{A}_x$)	0.50	0.22	0.32
λ_8 ($\hat{C}_x$)	0	-0.10	-0.16
Antisymmetric subspace			
λ_1 ($\hat{T}_{00}$)	0.01	-0.05	-0.04
λ_5 ($\hat{T}_{20}$)	0.01	0.02	0.02
λ_8 ($\hat{A}_x$)	-0.10	-0.05	-0.06
λ_9 ($\hat{C}_x$)	0	-0.03	-0.02

A4. Glossary

Long-lived states (LLS) refer to population imbalances with lifetimes $T_{LLS} > T_1$, usually imbalances between populations of states belonging to different irreducible representations of the spin permutation symmetry group, described by diagonal terms of the density matrix in the eigenbasis.

Long-lived coherences (LLC) refer to zero-quantum coherences with lifetimes $T_{LLC} > T_2$, which are coherences between states belonging to different irreducible representations, described by off-diagonal terms of the density matrix in the eigenbasis.

Separable or localized states refer to states in Hilbert space (there are 64 states in this work) that can be represented by direct products of eigenstates describing the spin pair *KK'* where *K* = *A, M* or *X*:

$$|\psi\rangle_{KK'} = c_1^{KK'}|S_0^{KK'}\rangle + c_2^{KK'}|T_{+1}^{KK'}\rangle + c_3^{KK'}|T_0^{KK'}\rangle + c_4^{KK'}|T_{-1}^{KK'}\rangle. \quad \text{(A2)}$$

A general form of a separable or localized state obtained for the 6-spin system is given by:

$$|\psi\rangle_{AA'}\otimes|\psi\rangle_{MM'}\otimes|\psi\rangle_{XX'} = \sum_i\sum_j\sum_k c_i^{AA'}c_j^{MM'}c_k^{XX'}\left|\psi_i^{AA'}\psi_j^{MM'}\psi_k^{XX'}\right\rangle. \quad \text{(A3)}$$

A separable state is a state which corresponds to a direct product of the pure states describing individual particles or subsystems. An example of such a state is $|T_0^{AA'}S_0^{MM'}S_0^{XX'}\rangle$ with the coefficients $c_3^{AA'} = c_1^{MM'} = c_1^{XX'} = 1$, while all remaining coefficients vanish.

Delocalized states refer to spin states in Hilbert space that *cannot* be obtained as a direct product of states $|\psi\rangle_{KK'}$ Eq. (A2), in analogy to delocalized linear combinations of atomic orbitals (LCAO's) that are familiar to chemists. This term here is synonymous to an inseparable and an entangled state. Examples of such states are given by states $|1'\rangle$, $|2'\rangle$, and $|3'\rangle$ of Eq. (19). This can be verified by considering the corresponding coefficients:

$$|1'\rangle = \frac{1}{2}\left(|S_0^{AA'}S_0^{MM'}T_0^{XX'}\rangle + \sqrt{2}|S_0^{AA'}T_0^{MM'}S_0^{XX'}\rangle + |T_0^{AA'}S_0^{MM'}S_0^{XX'}\rangle\right). \quad \text{(A4)}$$

From this equation it follows that localized states that could constitute such a state must have non-zero coefficients $c_1^{AA'}$, $c_3^{AA'}$, $c_1^{MM'}$, $c_3^{MM'}$, $c_1^{XX'}$, $c_3^{XX'}$. But at the same time, terms like $|S_0^{AA'}S_0^{MM'}S_0^{XX'}\rangle$ and $|T_0^{AA'}T_0^{MM'}T_0^{XX'}\rangle$ do not appear, meaning that some of these six coefficients must be zero. These two requirements are in direct conflict with each other, meaning that there is no set of states $|\psi\rangle_{AA'}$, $|\psi\rangle_{MM'}$, and $|\psi\rangle_{XX'}$ of which the direct product would produce the state $|1'\rangle$. We can therefore say that this state is neither localized nor separable.

Entanglement is easily evaluated in bipartite systems, or systems comprising two subsystems, but can be difficult in multipartite systems. In such systems, two subsystems can be chosen to evaluate entanglement [57]. For a system with three qubits, pairwise entanglement of qubits occurs for states like $|1'\rangle$ and $|3'\rangle$ [58].

Collective long-lived coherences refer to LLCs that comprise spins associated with nuclei belonging to different (not necessarily neighbouring) CH_2 groups.

Zero-quantum coherences refer to coherences between states that have the same total z-projection of the magnetic quantum number in the laboratory frame.

Precession refers to the evolution of coherences spanned between products of singlet and triplet states that may be delocalized.

Propagation refers to the interconversion of the coefficients of population imbalances between localized states. These imbalances can be associated with different CH_2 groups in the manner of **Fig. 8**. For example, the coefficients $\lambda_1(t)$ and $\lambda_2(t)$ in the density operator

$$\lambda_1(t)\left(|S_0S_0T_0\rangle\langle S_0S_0T_0| - \overline{|T_\iota T_J T_k\rangle\langle T_\iota T_J T_k|}\right) + \lambda_2(t)\left(|T_0S_0S_0\rangle\langle T_0S_0S_0| - \overline{|T_\iota T_J T_k\rangle\langle T_\iota T_J T_k|}\right) \quad \text{(A5)}$$

contains two terms that evolve so that $\partial\lambda_1(t)/\partial t = -\partial\lambda_2(t)/\partial t$ if relaxation is neglected.

Reconvertable refers to terms in Liouville space that can be reconverted into observable magnetization by single- or poly-SLIC.

Spin-chain refers (in this work) to a sequence of *n* pairs of CH_2 groups with states S_0 and T_0 (neglecting the states T_+ and T_-), where each pair of states S_0 and T_0 spans a two-level subsystem that can be described by a fictitious spin with spin quantum number I = ½. Such a chain bears analogies to one-dimensional chains of unpaired electron spins with $I = 1/2$. Such spin-chains (physical rather than fictitious) have been discussed for arbitrary *n*.

Spin-chain ZQ NMR refers to experiments that allow one to excite and observe specific LLSs and collective LLCs in an aliphatic chain $(CH_2)_n$.

References

[1] M. Carravetta, O. G. Johannessen, and M. H. Levitt, *Beyond the T1 Limit: Singlet Nuclear Spin States in Low Magnetic Fields*, Phys. Rev. Lett. **92**, 153003 (2004).

[2] M. Carravetta and M. H. Levitt, *Long-Lived Nuclear Spin States in High-Field Solution NMR*, J. Am. Chem. Soc. **126**, 6228 (2004).

[3] A. K. Grant and E. Vinogradov, *Long-Lived States in Solution NMR: Theoretical Examples in Three- and Four-Spin Systems*, J. Magn. Reson. **193**, 2 (2008).

[4] H. J. Hogben, P. J. Hore, and I. Kuprov, *Multiple Decoherence-Free States in Multi-Spin Systems*, J. Magn. Reson. **211**, 217 (2011).

[5] G. Pileio, editor , *Long-Lived Nuclear Spin Order* (The Royal Society of Chemistry, 2020).

[6] G. Pileio, M. Carravetta, and M. H. Levitt, *Extremely Low-Frequency Spectroscopy in Low-Field Nuclear Magnetic Resonance*, Phys. Rev. Lett. **103**, 083002 (2009).

[7] R. Sarkar, P. Ahuja, P. R. Vasos, and G. Bodenhausen, *Long-Lived Coherences for Homogeneous Line Narrowing in Spectroscopy*, Phys. Rev. Lett. **104**, 053001 (2010).

[8] K. F. Sheberstov, A. S. Kiryutin, C. Bengs, J. T. Hill-Cousins, L. J. Brown, R. C. D. Brown, G. Pileio, M. H. Levitt, A. V. Yurkovskaya, and K. L. Ivanov, *Excitation of Singlet–Triplet Coherences in Pairs of Nearly-Equivalent Spins*, Phys. Chem. Chem. Phys. **21**, 6087 (2019).

[9] A. Bornet, R. Sarkar, and G. Bodenhausen, *Life-Times of Long-Lived Coherences under Different Motional Regimes*, J. Magn. Reson. **206**, 154 (2010).

[10] R. Sarkar, P. Ahuja, P. R. Vasos, A. Bornet, O. Wagnières, and G. Bodenhausen, *Long-Lived Coherences for Line-Narrowing in High-Field NMR*, Prog. Nucl. Magn. Reson. Spectrosc. **59**, 83 (2011).

[11] A. S. Kiryutin, M. S. Panov, A. V. Yurkovskaya, K. L. Ivanov, and G. Bodenhausen, *Proton Relaxometry of Long-Lived Spin Order*, ChemPhysChem **20**, 766 (2019).

[12] F. Teleanu, A. Topor, D. Serafin, A. Sadet, and P. R. Vasos, *Rotating-Frame Overhauser Transfer via Long-Lived Coherences*, Symmetry **13**, 9 (2021).

[13] F. Teleanu, A. Ciumeica, O. Ianc, A. Lupulescu, A. Sadet, and P. R. Vasos, *Long-Lived Coherences for Magnetic Interactions in Proteins*, bioRxiv (2023).

[14] I. V. Zhukov, A. S. Kiryutin, A. V. Yurkovskaya, Y. A. Grishin, H.-M. Vieth, and K. L. Ivanov, *Field-Cycling NMR Experiments in an Ultra-Wide Magnetic Field Range: Relaxation and Coherent Polarization Transfer*, Phys. Chem. Chem. Phys. **20**, 12396 (2018).

[15] S. Bodenstedt, M. W. Mitchell, and M. C. D. Tayler, *Fast-Field-Cycling Ultralow-Field Nuclear Magnetic Relaxation Dispersion*, Nat. Commun. **12**, 1 (2021).

[16] A. Sonnefeld, G. Bodenhausen, and K. Sheberstov, *Polychromatic Excitation of Delocalized Long-Lived Proton Spin States in Aliphatic Chains*, Phys. Rev. Lett. **129**, 183203 (2022).

[17] J. A. Pople, W. G. Schneider, and H. J. Bernstein, *The Analysis of Nuclear Magnetic Resonance Spectra: Ii. Two Pairs of Two Equivalent Nuclei*, Can. J. Chem. **35**, 1060 (1957).

[18] M. C. D. Tayler and M. H. Levitt, *Paramagnetic Relaxation of Nuclear Singlet States*, Phys. Chem. Chem. Phys. **13**, 9128 (2011).

[19] B. Erriah and S. J. Elliott, *Experimental Evidence for the Role of Paramagnetic Oxygen Concentration on the Decay of Long-Lived Nuclear Spin Order*, RSC Adv. **9**, 40 (2019).

[20] A. Razanahoera, A. Sonnefeld, G. Bodenhausen, and K. Sheberstov, *Paramagnetic Relaxivity of Delocalized Long-Lived States of Protons in Chains of CH_2 Groups*, Magnetic Resonance Discussions 1 (2022).

[21] S. J. DeVience, R. L. Walsworth, and M. S. Rosen, *Preparation of Nuclear Spin Singlet States Using Spin-Lock Induced Crossing*, Phys. Rev. Lett. **111**, 173002 (2013).

[22] S. J. DeVience, R. L. Walsworth, and M. S. Rosen, *Probing Scalar Coupling Differences via Long-Lived Singlet States*, J. Magn. Reson. **262**, 42 (2016).

[23] W. Lenz, *Beitrag Zum Verständnis Der Magnetischen Erscheinungen in Festen Körpern.*, Z. Phys. **21**, 613 (1920).

[24] E. Ising, *Beitrag zur Theorie des Ferromagnetismus*, Z. Physik **31**, 253 (1925).

[25] F. Bloch, *Über die Quantenmechanik der Elektronen in Kristallgittern*, Z. Physik **52**, 555 (1929).

[26] R. Feynman, R. B. Leighton, and M. Sands, *15-1 Spin Waves*, in *The Feynman Lectures on Physics* (Addison–Wesley, 1964).

[27] R. Konrat, I. Burghardt, and G. Bodenhausen, *Coherence Transfer in Nuclear Magnetic Resonance by Selective Homonuclear Hartmann-Hahn Correlation Spectroscopy*, J. Am. Chem. Soc. **113**, 9135 (1991).

[28] Ē. Kupče and R. Freeman, *Stepwise Propagation of Coherence along a Chain of Atoms: DAISY-2*, J. Magn. Reson. (1969) **100**, 208 (1992).

[29] N. Khaneja and S. J. Glaser, *Efficient Transfer of Coherence through Ising Spin Chains*, Phys. Rev. A **66**, 060301 (2002).

[30] R. Marx and S. J. Glaser, *Spins Swing like Pendulums Do: An Exact Classical Model for TOCSY Transfer in Systems of Three Isotropically Coupled Spins 1/2*, J. Magn. Reson. **164**, 338 (2003).

[31] G. Schrumpf, *NMR Spectra of Monosubstituted Alkanes I. N-Propyl Derivatives*, J. Magn. Reson. (1969) **6**, 243 (1972).

[32] K. G. R. Pachler and P. L. Wessels, *Rotational Isomerism: V. A Nuclear Magnetic Resonance Study of 1,2-Diiodoethane*, J. Mol. Struct. **3**, 207 (1969).

[33] M. J. Minch, *Orientational Dependence of Vicinal Proton-Proton NMR Coupling Constants: The Karplus Relationship*, Concepts Magn. Reson. **6**, 41 (1994).

[34] W. P. Aue, E. Bartholdi, and R. R. Ernst, *Two-dimensional Spectroscopy. Application to Nuclear Magnetic Resonance*, J. Chem. Phys. **64**, 2229 (1976).

[35] A. Wokaun and R. R. Ernst, *Selective Detection of Multiple Quantum Transitions in NMR by Two-Dimensional Spectroscopy*, Chem. Phys. Lett. **52**, 407 (1977).

[36] L. Müller, *Mapping of Spin-Spin Coupling via Zero-Quantum Coherence*, J. Magn. Reson. (1969) **59**, 326 (1984).

[37] L. D. Hall and T. J. Norwood, *Zero-Quantum-Coherence Correlation Spectroscopy*, J. Magn. Reson. (1969) **69**, 585 (1986).

[38] J. Cavanagh and J. Keeler, *Multiplet Effects in Two-Dimensional Double-Quantum-Filtered Zero-Quantum Spectroscopy*, J. Magn. Reson. (1969) **77**, 612 (1988).

[39] N. Chandrakumar and F. Chandrasekaran, *Strongly Coupled Zero-Quantum Spectra*, J. Magn. Reson. (1969) **96**, 657 (1992).

[40] H. Günther, *NMR Spectroscopy: Basic Principles, Concepts and Applications in Chemistry, 2nd Edition | Wiley*, 2nd ed. (John Wiley & Sons, Ltd, Chichester, 1995).

[41] C. Bengs and M. H. Levitt, *SpinDynamica: Symbolic and Numerical Magnetic Resonance in a Mathematica Environment*, Magn. Reson. Chem. **56**, 374 (2018).

[42] L. D. Landau and E. M. Lifschitz, *Quantum Mechanics: Non-Relativistic Theory*, 3rd ed. (Pergamon Press, 1977).

[43] H. Eisendrath, W. Stone, and J. Jeener, *NMR of Protons in Gypsum. I. Experimental Proof of the Existence of Four Thermodynamic Invariants*, Phys. Rev. B **17**, 47 (1978).

[44] M. Goldman, *Interference Effects in the Relaxation of a Pair of Unlike Spin-12 Nuclei*, J. Magn. Reson. (1969) **60**, 437 (1984).

[45] A. Sonnefeld, A. Razanahoera, P. Pelupessy, G. Bodenhausen, and K. Sheberstov, *Long-Lived States of Methylene Protons in Achiral Molecules*, Sci. Adv. **8**, eade2113 (2022).

[46] A. S. Kiryutin, A. N. Pravdivtsev, A. V. Yurkovskaya, H.-M. Vieth, and K. L. Ivanov, *Nuclear Spin Singlet Order Selection by Adiabatically Ramped RF Fields*, J. Phys. Chem. B **120**, 11978 (2016).

[47] M. C. D. Tayler, *Chapter 10: Filters for Long-Lived Spin Order*, in *Long-Lived Nuclear Spin Order* (The Royal Society of Chemistry, 2020), pp. 188–208.

[48] M. Sabba, N. Wili, C. Bengs, J. W. Whipham, L. J. Brown, and M. H. Levitt, *Symmetry-Based Singlet–Triplet Excitation in Solution Nuclear Magnetic Resonance*, J. Chem. Phys. **157**, 134302 (2022).

[49] S. Wimperis, *Broadband, Narrowband, and Passband Composite Pulses for Use in Advanced NMR Experiments*, J. Magn. Reson. Ser. A. **109**, 221 (1994).

[50] F. Bloch and A. Siegert, *Magnetic Resonance for Nonrotating Fields*, Phys. Rev. **57**, 522 (1940).

[51] R. R. Ernst, G. Bodenhausen, A. Wokaun, R. R. Ernst, G. Bodenhausen, and A. Wokaun, *Principles of Nuclear Magnetic Resonance in One and Two Dimensions* (Oxford University Press, Oxford, New York, 1990).

[52] B. A. Rodin, K. F. Sheberstov, A. S. Kiryutin, L. J. Brown, R. C. D. Brown, M. Sabba, M. H. Levitt, A. V. Yurkovskaya, and K. L. Ivanov, *Fast Destruction of Singlet Order in NMR Experiments*, J. Chem. Phys. **151**, 234203 (2019).

[53] N. Salvi, R. Buratto, A. Bornet, S. Ulzega, I. Rentero Rebollo, A. Angelini, C. Heinis, and G. Bodenhausen, *Boosting the Sensitivity of Ligand–Protein Screening by NMR of Long-Lived States*, J. Am. Chem. Soc. **134**, 11076 (2012).

[54] R. Buratto, D. Mammoli, E. Chiarparin, G. Williams, and G. Bodenhausen, *Exploring Weak Ligand–Protein Interactions by Long-Lived NMR States: Improved Contrast in Fragment-Based Drug Screening*, Angew. Chem. Int. Ed. **53**, 11376 (2014).

[55] R. Buratto, D. Mammoli, E. Canet, and G. Bodenhausen, *Ligand–Protein Affinity Studies Using Long-Lived States of Fluorine-19 Nuclei*, J. Med. Chem. **59**, 1960 (2016).

[56] C. Bengs, L. Dagys, G. A. I. Moustafa, J. W. Whipham, M. Sabba, A. S. Kiryutin, K. L. Ivanov, and M. H. Levitt, *Nuclear Singlet Relaxation by Chemical Exchange*, J. Chem. Phys. **155**, 124311 (2021).

[57] L. Amico, R. Fazio, A. Osterloh, and V. Vedral, *Entanglement in Many-Body Systems*, Rev. Mod. Phys. **80**, 517 (2008).

[58] V. Coffman, J. Kundu, and W. K. Wootters, *Distributed Entanglement*, Phys. Rev. A **61**, 052306 (2000).